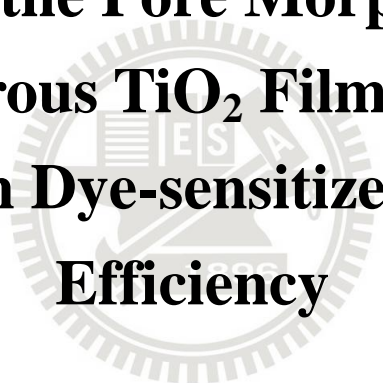


國立交通大學  
材料科學與工程學所  
碩士論文

微孔洞二氧化鈦薄膜孔洞形貌修飾及其  
對染料敏化太陽能電池效率之影響

**Tailoring the Pore Morphology of  
Mesoporous TiO<sub>2</sub> Films and Its  
Influence on Dye-sensitized Solar Cell  
Efficiency**



研究生：徐琬婷

指導教授：呂志鵬 博士

中華民國九十九年十二月

# **Tailoring the Pore Morphology of Mesoporous TiO<sub>2</sub> Films and Its Influence on Dye-sensitized Solar Cell Efficiency**

Student: Wan-Ting Hsu

Advisor: Dr. Jihperng Leu

Department of Materials Science and Engineering

National Chiao Tung University

## **Abstract**

Dye sensitized solar cell (DSSC) is one of leading technology to the next generation of solar cells. The porous TiO<sub>2</sub> working electrode plays an important key in DSSCs and affects the conversion efficiency. Specifically, the pore morphology of the TiO<sub>2</sub> film affects dye adsorption, electron transport, and electrolyte diffusion. In this study, in order to modify the pore morphology of TiO<sub>2</sub> (pore size, surface area, and porosity) to improve the DSSC performance, solvents and PEG in different molecular weights and loadings were added to TiO<sub>2</sub> paste, in addition to using different PEG burn out rate after TiO<sub>2</sub> films coating. In specific, TiO<sub>2</sub> films with different pore morphology were prepared by coating commercial TiO<sub>2</sub> nanoparticles (P25) and a scattering layer on FTO conducting glass using doctor-blade technique. The surface area, porosity, and pore size of TiO<sub>2</sub> films and the photochemical characteristics of DSSCs with these TiO<sub>2</sub> films were examined.

Results showed that PEG addition could separate the TiO<sub>2</sub> particles leading to modify the pore morphology of TiO<sub>2</sub>. In butanol based solvent, the surface area and porosity of TiO<sub>2</sub> film only increased slightly because butanol is a poor solvent for

PEG, and PEG molecules tend to curl in a poor solvent. Even changed the molecular weights, there was almost no difference of molecule sizes in the TiO<sub>2</sub> paste. When the solvent was changed from butanol to water, the average pore size was increased from 11.8 nm to 22 nm due to the large solubility of PEG leading full PEG chain extension in the TiO<sub>2</sub> particle matrix. And the molecular weights adjusting in water solution increased the pore size from 22 nm for 35k PEG to 30.5 nm for 100k PEG. Because the PEG porogen (pore generator) in good solvent (water) leading the polymer chains of PEG tend to extend well and attach onto TiO<sub>2</sub> particles, as the PEG polymer chains are fully extended in water-based TiO<sub>2</sub> paste, higher molecular weight shall lead to larger polymer coil size.

In addition to using different solvents and molecular weights of PEG, burn out rate is another issue to modify the pore morphology of TiO<sub>2</sub>. When an additional isothermal bake at 100°C the average pore size increased due to the expansion of PEG polymer chains and possibly some degree of PEG chain aggregation. In contrast, PEG chains were decomposed readily without enough time for chain extension. This yielded smaller pore size (11.8 nm for 35K PEG in butanol system, or 22.0 nm for 35k PEG in water system) under a fast burn-out rate at 400°C.

For DSSCs application, the conversion efficiency of DSSC increased with increasing pore size by PEG addition because larger pore size leading electrolyte diffuse more easily in the TiO<sub>2</sub> films led to faster dye regeneration, and the electron transport resistance in the TiO<sub>2</sub>/dye/electrolyte interface ( $R_2$ ) and the resistance ( $R_3$ ) of Nernstian diffusion decreased. In this study, the best conversion efficiency of DSSC reached 5.13% with open circuit voltage 0.73V and short circuit current density 13.07mA/cm<sup>2</sup>. TiO<sub>2</sub> electrode of this DSSC was prepared by 15% 35k PEG loading TiO<sub>2</sub> paste in water system and the average pore size was 22 nm.

# 微孔洞二氧化鈦薄膜孔洞形貌修飾及其對染料敏化太陽能電池效率之影響

研究生：徐琬婷

指導教授：呂志鵬 博士

國立交通大學材料科學與工程學系碩士

## 摘要

染料敏化太陽能電池(Dye-sensitized solar cell, DSSC)是目前極具發展潛力的新一代有機太陽能電池。其中，奈米孔洞二氧化鈦電極扮演著重要的角色，是影響染料敏化太陽能電池轉換效率的關鍵之一。具體來說，奈米孔洞結構二氧化鈦薄膜的對染料的吸附、電子傳輸、電解質擴散等皆有其影響。在這項研究中，利用在二氧化鈦漿料中添加不同分子量的聚乙二醇(polyethylene glycol, PEG)及溶劑，以及不同的聚乙二醇燒除速度修飾二氧化鈦薄膜的孔洞大小和孔隙率。另外，修飾後的二氧化鈦薄膜將封裝成染料敏化太陽能電池，並進一步量測其光電轉換效率及電池內電阻。

二氧化鈦漿料在加入聚乙二醇後，其製備成的二氧化鈦薄膜有較大的比表面積、孔洞大小及孔隙率。若所使用的二氧化鈦漿料為去離子水或以緩慢的速度燒除聚乙二醇，二氧化鈦薄膜的孔洞大小及孔隙率將成會更大。且在聚乙二醇的添加後，二氧化鈦薄膜的孔洞大小分佈則是一雙峰分佈。利用上述方式可以控制二氧化鈦膜的孔洞大小由 8.07 nm 增加至 35.13 nm，而孔隙率由 31.05% 增加至 69.81%。

將二氧化鈦多孔薄膜製備成染料敏化太陽能電池之後可以發現，二氧化鈦多孔電極中具有較大的比表面積可以吸附更多的染料，較大的孔洞大小及孔隙率可

以讓電解液擴散更容易，導致更快的染料再生和高的光電轉換效率。增加二氧化鈦多孔電極中的孔洞大小及孔隙率後，染料敏化太陽能電池的光電轉換效率從 4.31% 上升至 5.13%。電化學阻抗譜 (Electrochemical impedance spectrum, EIS) 分析後可得知，在二氧化鈦/染料/電解質介面上的電子傳遞阻力( $R_2$ )和電解液的擴散電阻( $R_3$ )的隨孔洞大小及孔隙率增加而增加。此結果可以再次確認從電池效率分析後所得到的結論。

最佳化的奈米孔洞二氧化鈦電極是由添加了 15% 的聚乙二醇(分子量 35,000) 的水系二氧化鈦漿料所製備的，其比表面積為  $59.12\text{m}^2/\text{g}$ ，平均孔洞大小為  $22.07\text{nm}$ ，孔隙為 50.87%。以此電極所組成的染料敏化太陽能電池能達到 5.13% 的光電轉換效率，而其填充因子為 0.54，開路電壓為 0.73V，短路電流密度則是  $13.07\text{mA}/\text{cm}^2$ 。



## Acknowledgement

很高興在碩士班期間可以加入呂志鵬教授實驗室這個大家庭，在這裡與大家一起努力。要先感謝呂志鵬老師在各方面的指導，除了學術研究之外，也學習到了許多科技寫作與報告呈現的技巧。另外在做人處事及未來在職場上所應具備的能力，也在這期間曾進不少，十分感謝老師的用心與叮嚀。

實驗室的學長姐也在這些日子裡給予大力的幫助，讓我備感溫馨。要先謝謝國原學長，在這段期間給予的許多幫助和實驗資源。謝謝幸鈴學姊，在專業的化學領域給了我很大的幫助，當我遇到困難時，總能幫助我找到最佳的解決方法。感謝明義學長，在學長的細心帶領下，學會了很多實驗設計及實驗結果的分析討論方法。還有實驗室的各位學長姐，經常陪我聊天的王智學長，總為我帶來愉快心情的邱詩雅學姐，有趣可愛的車牧龍學長，風趣幽默的大龜學長還有弘恩學長。感謝他們親切的帶領我學習研究時所需的各項能力，提供我專業的意見，或是日成生活中的幫助。

謝謝我的同學伯政和瑜修，在平時跟我討論課業或陪我說話。可以有像他們這樣的同學可以相互鼓勵學習是很令人開心的事。還有實驗室的學弟妹們，書豪、沁穎、奎岳、勝翔還有田丞芳，很感謝他們聽我抱怨，在日常生我中也幫了我一些忙。很感謝大家，讓我在這些時間學習到很多，得到很多，也過得很充實。最後要感謝我的家人，因為他們的支持，我才能無憂的完成碩士學位，感謝他們的付出與諒解。

# Contents

Abstract.....	I
摘要.....	III
Acknowledgement .....	V
Contents .....	VI
Figure Captions.....	VIII
Table Captions .....	X
Chapter 1 Introduction .....	1
Chapter 2 Literature Review .....	5
2.1 Dye-sensitized Solar Cell.....	5
2.1-1 DSSC Structure Analysis and Working Principle.....	5
2.1-2 Operation Principles of Dye-sensitized Solar Cells .....	8
2.2 Components of DSSCs .....	10
2.2-1 Substrate .....	10
2.2-2 Nanocrystalline Photo-anode.....	10
2.2-3 The Sensitizer: Organic dye.....	12
2.2-4 Electrolyte.....	15
2.2-5 Counter electrode.....	18
2.2-6 Sealant and Spacer.....	19
2.2-7 Post-treatment/Pretreatments/Underlayer.....	20
2.3 TiO <sub>2</sub> morphology control .....	22
2.3-1 Different TiO <sub>2</sub> Particle Size.....	22
2.3-2 Muti-Layer of TiO <sub>2</sub> Film .....	23
2.3-3 TiO <sub>2</sub> Nanotube .....	24
2.3-4 Special TiO <sub>2</sub> Nanostructure .....	24
2.3-5 Dispersive Polymer Addition.....	26
2.4 Instrument Methodologies .....	28
2.4-1 Brunauer–Emmett–Teller .....	28
2.4-2 Electrochemical Impedance Spectroscopy (EIS) .....	30
Chapter 3 Experimental Section .....	33
3.1 Materials .....	33
3.2 TiO <sub>2</sub> Paste Preparation .....	35
3.2-1 TiO <sub>2</sub> paste composition.....	35
3.2-2 TiO <sub>2</sub> paste mixing process .....	36
3.3 TiO <sub>2</sub> film Preparation.....	37
3.4 DSSCs fabrication.....	39
3.5 Characterization Techniques .....	41

3.5-1 Brunauer–Emmett–Teller (BET) Analysis .....	41
3.5-2 Scanning Electron Microscopy (SEM).....	41
3.5-3 Uv-Visible Light Spectrum .....	41
3-5-4 Phtocurrent Examination.....	42
3-5-5 Electrochemical Ipedance Sectroscopy (EIS) .....	42
3.6 Experimental Flow .....	43
Chapter 4 Results and Discussion.....	44
4.1 Characterization of TiO <sub>2</sub> films .....	44
4.1-1 Surface morphology and film thickness of TiO <sub>2</sub> film.....	44
4.1-2 Pore Morphology of TiO <sub>2</sub> Film .....	46
4.1-2.1 Effects of PEG Molecular Weight and Loading on Pore Morphology of TiO <sub>2</sub> Films .....	49
4.1-2.2 Effect of solvents on Pore Morphology of TiO <sub>2</sub> Films.....	52
4.1-2.3 Effect of PEG Burn-out Rate on the Pore Morphology of TiO <sub>2</sub> Films .....	58
4.1-3 Dye Adsorption Analysis .....	63
4.2 DSSC performance .....	67
4.2-1 Cell Efficiency .....	67
4.2-2 Impedance inside DSSCs.....	72
Chapter 5 Conclusion.....	78
Reference .....	80



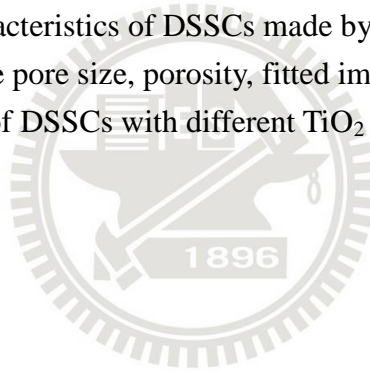
## Figure Captions

Fig. 1- 1 The path length, in units of Air Mass, changes with zenith angle.....	2
Fig. 2- 1 The structure of DSSC .....	5
Fig. 2- 2 Schematic of operation of DSSC .....	6
Fig. 2- 3 Spectral response curve of the photocurrent for the DSSC sensitized by N3 and the black dye. The chemical structure of N3 dye and black dye.....	13
Fig. 2- 4 The chemical structure of N719 dye and N749 (black dye). .....	14
Fig. 2- 5 Structure of the ruthenium sensitizers RuL <sub>3</sub> (yellow) <i>cis</i> -RuL <sub>2</sub> (NCS) <sub>2</sub> (red) and RuL (NCS) <sub>3</sub> (green) where L) 2,2'-bipyridyl-4,4'-dicarboxylic acid and L) 2,2',2''-terpyridyl -4,4',4''-tricarboxylic acid. The lower part of the picture shows nanocrystalline TiO <sub>2</sub> films loaded with a monolayer of the respective sensitizer. .....	14
Fig. 2- 6 An Ideal Nyquist Plot .....	31
Fig. 2- 7 The equivalent circuit for the DSSCs with liquid type electrolyte .....	32
Fig. 3- 1 Coating process of the TiO <sub>2</sub> film. (a) Doctor-blade coating TiO <sub>2</sub> film. (b) TiO <sub>2</sub> film sintered at 400°C. (c) Spin-coating scattering layer. (d) TiO <sub>2</sub> electrode sintered at 400°C. ....	38
Fig. 3- 2 The DSSC fabrication process. (a) Sealing the dye-sensitized photoanode and Pt-coated counter electrode. (b) Electrolyte injection. (c) Sealing the electrolyte injection holes on counter electrode.....	40
Fig. 3- 3 Experiment Design chart.....	43
Fig. 4-1 The surface morphology and film thickness of TiO <sub>2</sub> electrodes prepared at various PEG loadings (5, 10, 15, and 20%) (a)-(d): surface morphology; (e)-(h): TiO <sub>2</sub> film thickness .....	45
Fig. 4-2 SEM image of (a) scattering layer (100 nm TiO <sub>2</sub> particles) coated on TiO <sub>2</sub> film (21 nm TiO <sub>2</sub> particle) (X4,000) and (b) under large magnification (X40,000). .....	46
Fig. 4-3 N <sub>2</sub> adsorption-desorption standard isotherms for (a) micro-porous sample, (b) non-porous sample, (c) macro-porous sample, (d) meso-porous sample, (e) micro-porous or meso-porous sample and (f) sample with pores more than one type. [109].....	47
Fig. 4-4 The N <sub>2</sub> adsorption-desorption isotherms of the TiO <sub>2</sub> films prepared by TiO <sub>2</sub> paste in (a) butanol solution and (b) water solution.....	48
Fig. 4-5 A bimodal pore size distribution of the TiO <sub>2</sub> film prepared by paste using	

15% PEG (MW = 100k) loading and H <sub>2</sub> O solvent .....	49
Fig. 4-6 The pore size distributions of the TiO <sub>2</sub> film produced by TiO <sub>2</sub> paste with 35k and 100k PEG addition and in different solvent system.....	51
Fig. 4-7 The pore size distributions of the TiO <sub>2</sub> film produced by TiO <sub>2</sub> paste with 35k PEG in different solvent system. ....	53
Fig. 4-8 Average pore size and porosity of TiO <sub>2</sub> films using different solvent systems .....	55
Fig. 4-9 Schematic diagram of PEG working mechanism in TiO <sub>2</sub> paste with different solvent systems. (a) TiO <sub>2</sub> film without PEG loading, (b) TiO <sub>2</sub> film with PEG loading in butanol solution, and (c) TiO <sub>2</sub> film with PEG loading in water solution.....	57
Fig. 4-10 Average pore size and porosity of TiO <sub>2</sub> films with different PEG molecular weight.....	58
Fig. 4-11 The pore size distributions of the TiO <sub>2</sub> film prepared by different PEG burn-out rates using water-based pastes. ....	59
Fig. 4-12 (a) Average pore size and porosity of TiO <sub>2</sub> films with different PEG burn-out rates in butanol system (b) in water system .....	60
Fig. 4-13 UV-visible spectra of the reference dye solution and the dye desorption solution of TiO <sub>2</sub> film prepared by TiO <sub>2</sub> paste with 35k PEG loading in butanol system. ....	65
Fig. 4-14 Dye adsorption and surface area of TiO <sub>2</sub> films as a function of pore size ...	65
Fig. 4-15 I-V curve of DSSC with TiO <sub>2</sub> electrode prepared by PEG (35k, 15% loading) TiO <sub>2</sub> paste in butanol system. ....	68
Fig. 4-16 I-V curves of DSSCs with TiO <sub>2</sub> electrode prepared by TiO <sub>2</sub> paste with no PEG loading, 35k PEG 15% loading in water system, and 100k PEG 15% loading in water system combined with slow PEG burn-out process.....	69
Fig. 4-17 An EIS spectrum (Nyquist diagram) of DSSC with TiO <sub>2</sub> electrode prepared by PEG (35k, 15% loading)-water paste under illumination.....	73
Fig. 4-18 The equivalent circuit for the DSSC .....	73
Fig. 4-19 EIS spectra of DSSC with TiO <sub>2</sub> electrode prepared by TiO <sub>2</sub> paste with (1) no PEG loading, (2) PEG (35k, 15% loading) in water system, and (3) PEG (100k, 15% loading) in water system combined with a slow PEG burn-out process. ....	74
Fig. 4-20 R <sub>2</sub> , R <sub>3</sub> and efficiency of DSSCs with different pore size TiO <sub>2</sub> films .....	76
Fig. 4-21 R <sub>2</sub> , R <sub>3</sub> and efficiency of DSSCs with different porosity TiO <sub>2</sub> films.....	77
Fig. 4-22 R <sub>2</sub> , R <sub>3</sub> and efficiency of DSSCs with different surface area TiO <sub>2</sub> films .....	77

## Table Captions

Table 3- 1 TiO <sub>2</sub> paste composition in butanol solution.....	35
Table 3- 2 TiO <sub>2</sub> paste composition in water solution.....	36
Table 4-1 Pore morphology of TiO <sub>2</sub> film prepared by PEG with various molecular weights and loadings in butanol system paste. ....	51
Table 4-2 Pore morphology of TiO <sub>2</sub> films prepared by PEG (15% loading; MW=35k or 100k) in different solvents.....	54
Table 4-3 Pore morphology of TiO <sub>2</sub> film prepared by PEG with various molecular weights and loading in butanol and water solvent systems and different PEG burn-out rates .....	62
Table 4-4 Average pore size, UV-visible absorption intensity, dye adsorption, and specific surface area of various TiO <sub>2</sub> films.....	66
Table 4-5 Photovoltaic characteristics of DSSCs made by different TiO <sub>2</sub> electrodes.	71
Table 4- 6 TiO <sub>2</sub> film average pore size, porosity, fitted impedance parameters and conversion efficiency of DSSCs with different TiO <sub>2</sub> electrodes.....	75



## Chapter 1 Introduction

After industrial revolution, energy consumption sharp increased and each kind of energy was developed one after another especially fossil fuel since 19<sup>th</sup> century. However, these energy source storages are limited and going to be exhausted this century. Also, the highly usage of fossil fuel caused serious environmental pollution and ecological damage. United Nation Framework Convention on Climate Change (UNFCCC) and Kyoto Protocol clearly emphasize the importance of renewable energy development.

Renewable energy including waterpower, wind power, solar, biologic energy, terrestrial heat, ect. and these energy can transfer into electric power, heat, chemical power and fuel. In all kinds of energy, solar energy is almost inexhaustible and without environment pollution. The supply of energy from the Sun to the Earth is gigantic:  $3 \times 10^{24}$  joules a year, or about 10,000 times more than the global population currently consumes, which means converting 0.1% of the Earth's surface with solar cells with an efficiency of 10% would theoretically satisfy our present needs. [1]

Nevertheless, the solar energy from the sun cannot be use efficiently. Part of the sun power would be absorbed by the Earth's atmosphere or reflected to space. The Air Mass (AM) value is set to describe the spectrum (not necessarily the intensity) of sunlight at particular latitude. It is defined as the distance through the atmosphere that the light from the sun travels in order to reach the solar cell. This is expressed relative to conditions at the equator, where the sun is almost directly overhead, and where the light is therefore described as AM1.0. Thus in space, without atmosphere, the spectrum is referred to as AM0.

For most terrestrial applications, the generally accepted solar cell testing

standard is that of AM1.5 conditions. In addition, we usually also specify the intensity of the light, integrated over the spectrum, as being  $100\text{mW/m}^2$  (1 sun). When using solar concentrators, such as the intensity might be increased by a factor of 1000, but the shape of the spectrum would remain AM1.5. [2]

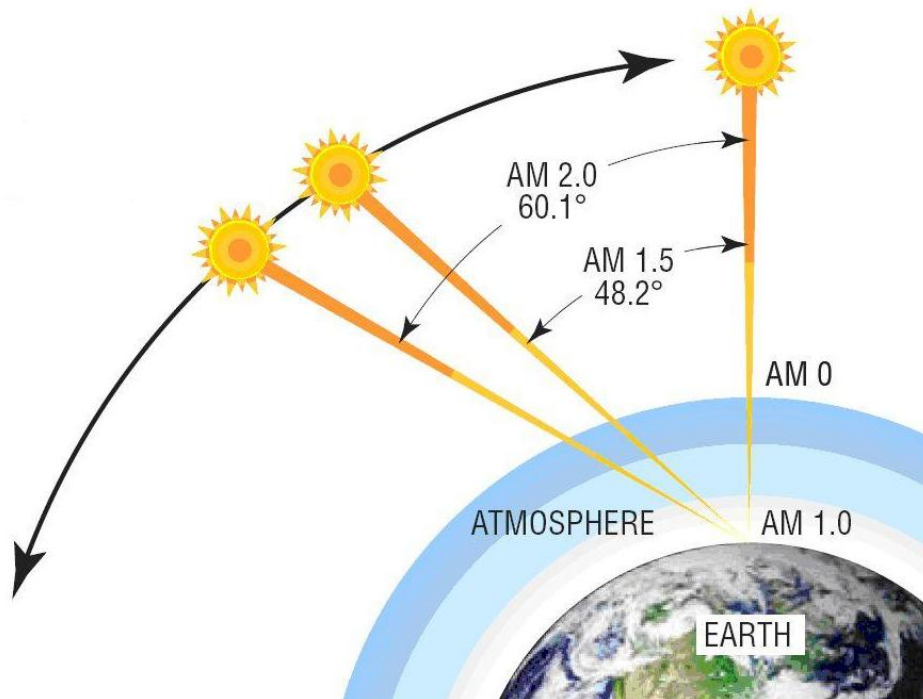


Fig. 1-1 The path length, in units of Air Mass, changes with zenith angle. [3]

Even though the sun energy is hard to be used efficiently, solar power still offers a realistic solution to energy problems and that is the reason solar cells have attracted extensive attention and fast developed. Solar can be transformed to electricity, fuels and heat through varied solar utilization, without noise and it produces no air pollution. Massive solar power conversion would ensure abundant energy and safe clear environment for future generations.

In all kinds of solar cells, silicon (Si) base solar cells are more mature developed and main products on the market. However, the coast of silicon base solar cells is higher than other energy generation method and only be used at specific situation. It is

important to development more low cost and high conversion efficiency solar cells for mass energy generation for popular use.

Gratzel *et al.* developed a new kind of solar cell, dye-sensitized solar cell, which has relatively high conversion efficiency, simple fabrication process, low production cost and transparency in 1991. [4] Great conversion efficiencies (above 11%) have been reported based on mesoporous nanocrystalline TiO<sub>2</sub> film, ruthenium sensitized dye, triiodide/iodide redox couple in organic solvent as the electrolyte and platinum coated counter electrode. [5, 6] Because its easy production process and transparency can be design to combine with various electronic device and become portable final products.

The performance and efficiency of the DSSC depend on many factors such as the platinum layer of the counter electrode, the TiO<sub>2</sub> layer surface morphology and the structure, dye molecules, the status and component of the electrolyte and so on. Mesoporous nanocrystalline TiO<sub>2</sub> films provide large surface area for dye adsorption, electrical connection with the redox electrolyte, electron diffusion and transportation. As the pore size and porosity of the TiO<sub>2</sub> film increases, the diffusion of electrolyte becomes easier, but the effective surface area decrease and the amount of dye adsorb less. Therefore, the morphology of the TiO<sub>2</sub> film plays a very important role in the high efficiency DSSC. There is a precise balance between pore size, porosity, effective surface area and thickness of TiO<sub>2</sub> film to achieve optimum DSSC performance.

Different shape and size of TiO<sub>2</sub> particles were used to fabricate high efficiency DSSCs. The use of small TiO<sub>2</sub> particles and large pore size was reported to yield good electron transport and high current efficiency of DSSCs. [7] Recently, TiO<sub>2</sub> nanotubes [8, 9] are introduced to enhance conversion efficiency for DSSCs due to its increased surface area for dye absorption. However, the syntheses of TiO<sub>2</sub> nanotubes or special

shape  $\text{TiO}_2$  are time-consuming multistep process, which is difficult to scale up for production. In contrast, a simple and efficient method to control the  $\text{TiO}_2$  film morphology is to add dispersive polymer into  $\text{TiO}_2$  paste to form larger pores, higher porosity, and more surface area. [10, 11] Most commonly used dispersive polymers are polyethylene glycol (PEG) and polystyrene. Some reports show the relationship between dispersive polymer addition and their effect on  $\text{TiO}_2$  characteristic [12-14]. However, there are only few reports talking about the dispersive polymer addition effect on the porosity and pore size in  $\text{TiO}_2$  films, resistances inside DSSCs and the cell performance.

In this study, for modifying the pore size and porosity of  $\text{TiO}_2$ , different molecular weight PEG and solvent were used in  $\text{TiO}_2$  paste and different PEG burn out rate were applied after  $\text{TiO}_2$  films coating.  $\text{TiO}_2$  films with different pore size and porosity were prepared by coating commercial  $\text{TiO}_2$  nanoparticles (P25) on FTO conducting glass using doctor-blade technique. Applying PEG and different solvents in  $\text{TiO}_2$  paste is an easy way to control the  $\text{TiO}_2$  film pore morphologies without change any process in produce DSSCs. The porosity and pore size of  $\text{TiO}_2$  films and the photochemical characteristics of DSSCs with these  $\text{TiO}_2$  films were investigated. The correlation between  $\text{TiO}_2$  film pore morphologies and DSSC performance were discussed. Finally, the pore morphology of  $\text{TiO}_2$  film was optimized for the best performance of DSSC.

## Chapter 2 Literature Review

### 2.1 Dye-sensitized Solar Cell

Brin O'Rengan and Michael Gratzel propose a high efficiency photovoltaic cell with  $\text{TiO}_2$  nanoporous film as semiconductor electrode, ruthenium (Ru) organometallic compound as light sensitizer and suitable redox couple solution as electrolyte [4]. This solar cell called "dye-sensitized solar cell" which had 7.1% conversion efficiency under sun illumination. A break through at 1999, the cell conversion efficiency reached 10% [15] and the best record of DSSC conversion efficiency is higher than 11.7%.

#### 2.1-1 DSSC Structure Analysis and Working Principle

Fig. 2-1 is the structure of DSSC. DSSC is a sandwich structure consist of TCO glass, dye sensitized  $\text{TiO}_2$  layer, electrolyte and platinum coated counter electrode.

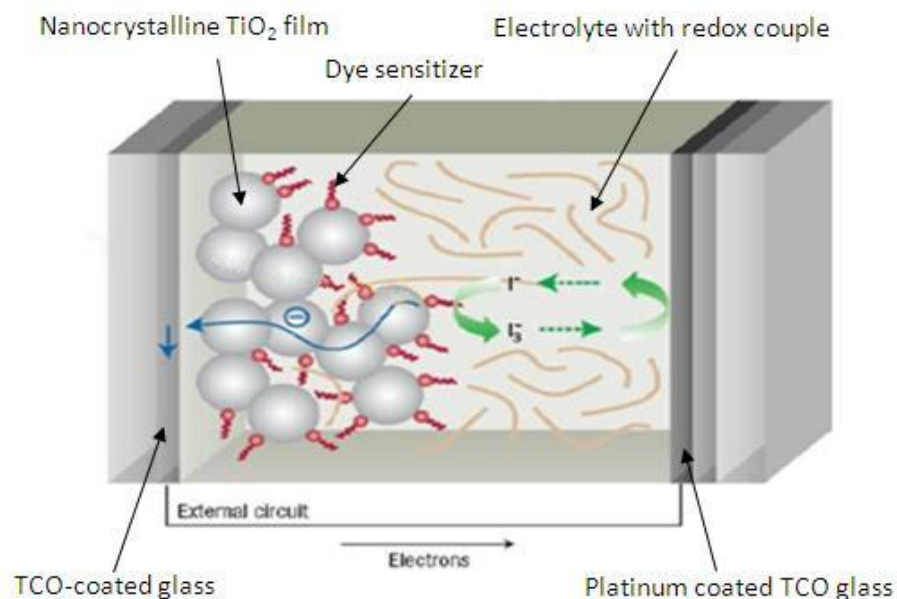


Fig. 2-1 The structure of DSSC [16]



Fig. 2-2 demonstrates the schematic structure of DSSC. The photoanode, which is made of mesoporous dye-sensitized semiconductor, receives electrons from the photo-excited dye which is oxidized. The oxidized dye molecules then turn to oxidize the mediator, the redox species in the electrolyte and regenerate dye. The mediator is regenerated by the reduction at the cathode by the electrons circulated through the external.

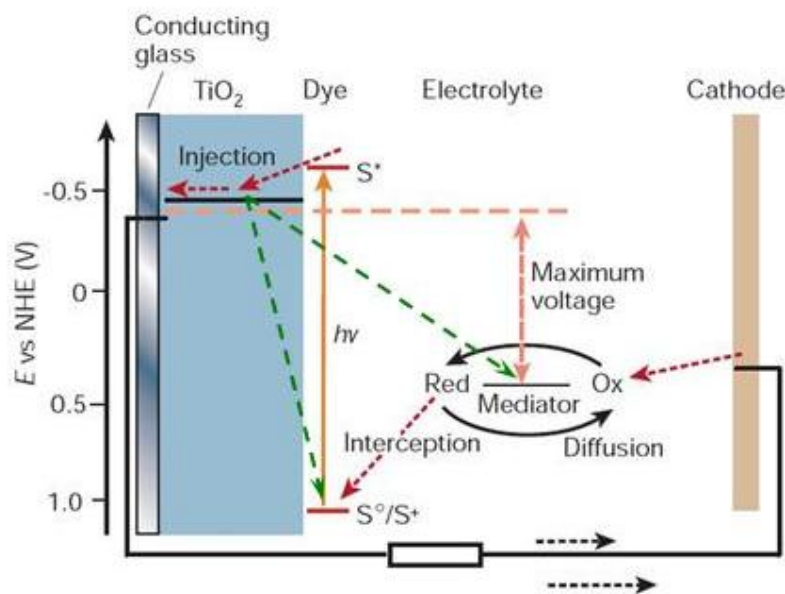


Fig. 2-2 Schematic of operation of DSSC [1]

1. Photoexcitation on dye molecules to induce charge separation:



2. Charge (electron) injects into conduction band of mesoporous  $TiO_2$ :



3. Charge passes through outer circuit via electronic load:



4. Dye reduces to ground state by redox couple in the electrolyte:



5. Redox couple reduces on counter electrode by the charge comes from outlet circuit:



The Total Reaction:



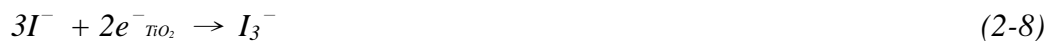
The TiO<sub>2</sub> mesoporous electrode does not work as the main light absorption character, but used a carrier transport host material inside DSSC systems. The synthesized organic dye attached to TiO<sub>2</sub> absorbs almost the visible light and made carrier injected from excited dye molecules then quickly transport to the current collector and then the outer circuit. It avoids the direct charge recombination, which is the energy-favored process after charge separation. The electrons and holes run different routes back to their ground state; this important property contributes to the unusual charge separation efficiency inside DSSC systems.

There are also some reasons make low DSSC conversion efficiency, such as electron/hole recombination inside DSSC, resistance of the materials and impedance at each material interface. The main recombinations are at TiO<sub>2</sub>/dye interface and TiO<sub>2</sub>/electrolyte interface, which might cause photocurrent loss.

Equation of recombination at TiO<sub>2</sub>/dye interface:



Equation of recombination at TiO<sub>2</sub>/electrolyte interface:



The resistance of row materials are decided when the material was chosen, but the impedance at each interface can be reduced by surface modification and post-treatment to improve the connection of each materials.

## 2.1-2 Operation Principles of Dye-sensitized Solar Cells

### 1. Open Current Voltage ( $V_{OC}$ ) Characteristics

When photovoltaic devices are under illumination, the open circuit voltage can be calculated from the diode equation. [5]

$$V_{OC} = \frac{nRT}{F} \ln \left( \frac{i_{sc}}{i_0} - 1 \right) \quad (2-9)$$

Where  $n$  is the ideality factor whose value is between 1 and 2 for DSSC, and  $i_0$  is the reverse saturation current, which can be measured in reasonably large reverse voltage. The two main characteristic quantities, the open circuit voltage  $V_{OC}$  which represents the voltage produce in the absence of any current, and short circuit current  $I_{SC}$  which stands for the current with no voltage across the cell.

When photovoltaic device are in dark, they should obey the ideal diode equation:

$$I = I_{sc} \left( e^{qV/kT} - 1 \right) \quad (2-10)$$

which indicates a positive applied voltage can make an easy current flow.

### 2. Incident Photons to Current Conversion Efficiency (IPCE)

IPCE is an important parameter when determining the performance of a photovoltaic device. IPCE is defined as the number of electrons flowing through the external circuit over the number of photons incident on the cell surface at a particular wavelength, which means IPCE the ratio of the observed photocurrent over the incident photon flux.

### 3. Cell Efficiency ( $\eta$ )

We called  $V_{OC}$  as the maximum voltage at photovoltaic device, and  $I_{SC}$  as the maximum short circuit current under illumination. The IV-curve yielding the maximum power is called  $P_{MAX}$ . In addition, another important parameter of cell

performance is the Fill Factor (FF), which is defined as follows:

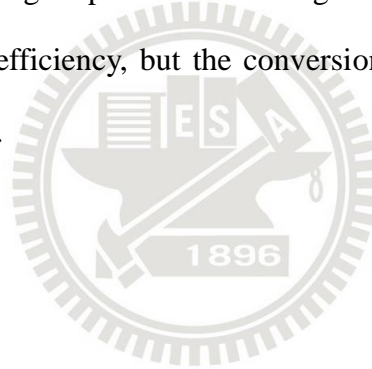
$$FF = \frac{P_{MAX}}{V_{OC} \times I_{SC}} \quad (2-11)$$

FF is an efficiency factor, used for checking whether the  $P_{MAX}$  is ideally equal to  $V_{OC} \times I_{SC}$  or not, because there are many impedances, including the contact resistance, electrolyte resistance, charge transfer resistance, ect. inside the cell to cause potential drop.

The overall energy conversion efficiency ( $\eta$ ) is defined to be the maximum power generated by DSSC under illumination:

$$\eta_{eff} = \frac{P_{MAX}}{P_{ill}} \times 100\% = \frac{V_{OC} \times I_{SC} \times FF}{P_{ill}} \times 100\% \quad (2-12)$$

Equation (2-10) indicates high open circuit voltage and short circuit current are necessary for high overall efficiency, but the conversion efficiency will still be low without high fill factor (FF).



## 2.2 Components of DSSCs

### 2.2-1 Substrate

The most used substrates for DSSC are transparent conducting oxide (TCO), the coated glass substrates. The choice of TCO coated glass is usually a compromise between transmittance and conductance. Fluorine-doped tin oxide, the  $\text{SnO}_2 \cdot \text{F}$  or FTO and indium tin oxide, or ITO are the most commonly used TCOs for thin film photovoltaic cells.[17] The reason choosing TCO coated glass substrates is for the procedure of  $\text{TiO}_2$  electrode including sintering and deposited film at 400- 500°C. FTO coated glass is the best choice for such high temperature process, although ITO can be more easily produced and is more inexpensive.

For meeting the trend of consumer electronic devices, recently a new focus of DSSC technology is directed to the realization of lightweight plastic film-type cells. For this purpose, replacement of TCO coated solid glass substrates with flexible plastic substrates has been the subject of intense study. The use of flexible substrates also brings about a significant merit for drastic cost reduction by manufacturing the entire cell through roll-to roll assembling. [18]

### 2.2-2 Nanocrystalline Photo-anode

For adsorption more dye molecules to increase the cell efficiency, high surface mesoporous semiconductor for DSSC become very important. Titanium dioxide is the fundamental semiconductor for DSSC because of its non-toxic properties, easy produce process, high stability and low cost. The surface is composed of 15-20nm-sized particles, and about 100 times the geometric area occupied for each micrometer of thickness. A roughness factor, defined as the ratio of the real surface area to the projected area, is at least 1000 to ensure efficient solar light harvesting by

the currently used sensitizers.[19] The thickness of TiO<sub>2</sub> film is typically 5-20μm and analysis of the layer morphology shows the porosity to be ~50-65%.

There are two main ways to prepare TiO<sub>2</sub> photoanode. One is the “sol-gel method”[20, 21], by which TiO<sub>2</sub> is prepared from hydrolysis of Ti-alkoxides and addition of binder. Narrow particle size distribution and fine-ordered crystal structure can be obtained by carefully controlling every preparing step. However, this method is limited to small scale for laboratory only although these properties are desired in standard electrode. The other one is “paste-coating method”[22, 23], by which commercial TiO<sub>2</sub> nanoparticles such as Degussa P25 and the binder are to maintain the dispersion, which could be the convenient way producing TiO<sub>2</sub> photoelectrodes. The morphology control of TiO<sub>2</sub> film is also important for photoanode which is reviewed in next section.

The above two well-mixed paste is applied to TCO substrate by (1) Doctor Blade Method, (2) Screen Printing and (3) Spin Coating techniques. After coating and air-drying, the film is then sintered at 450-500°C for 30 minutes in order to decompose organic binders and surfactants and to improve electrical contact between adjacent TiO<sub>2</sub> particles in the porous layer as well as between the TiO<sub>2</sub> particles and substrate at the same time.

There are still other ways for preparing nanostructured TiO<sub>2</sub> electrodes, including electrodeposition [24-26], evaporation [27], sputter deposition[28-32], chemical vapor deposition [33, 34], ect. Other methods use highly-ordered TiO<sub>2</sub> nanotube arrays [35] and mixture of TiO<sub>2</sub> nanowires and nanoparticles [36] as photoelectrode. Both front-side and back-side illumination were applied when using the TiO<sub>2</sub> nanotube arrays electrode, indicating that electron transport in the nanotube is faster than between nanoparticles.

### 2.2-3 The Sensitizer: Organic dye

As mentioned before, the organic dye becomes a sensitizer which absorbs most of the incident light and increases the cell efficiency. Organic dye used in photoelectrochemical cells should meet the follow needs:

1. Absorption: With good absorption in visible light region up to wavelength 920nm, almost the incident light from sun.
2. Energetic: With sufficient electrons on excited state providing the driving force to make electrons inject to conduction band of TiO<sub>2</sub> thin film. Organic dye should also have relative low ground state for reduction by the redox couple in electrolyte.
3. Kinetics: The rate of electron injection should be high, and the lifetime of excited electrons should be long enough.
4. Stability: The organic dye can be operated under normal environment for more than 10<sup>8</sup> times of the redox cycle reaction and can be operated for more 20 years.
5. Interfacial Properties: It can attach on TiO<sub>2</sub> surface and not easily desorption from TiO<sub>2</sub> electrode.

A breakthrough of organic sensitized dye is accomplished by Gratzel's group at EPFL in Switzerland by using metallo-organic ruthenium complex as the "dye" along with nanostructured TiO<sub>2</sub> electrode.[4] The dye have the general structure ML<sub>2</sub>(X)<sub>2</sub>, where L stands for 2,2'-bipyridyl-4,4'-dicarboxylic acid, M for ruthenium or osmium and X for halide, cyanide, thiocyanate. The cis-RuL<sub>2</sub>(NSC)<sub>2</sub>, also called N3 dye has shown impressive performance and has been wide used in DSSC research. Fig. 2-3 compares the spectral response of the photocurrent observed with two sensitizers. The incident photo to current conversion efficiency (IPCE) of DSSC is plotted as a function of excitation wavelength. Both chromophores show high IPCE values in the

visible range. However, the response of the black dye extends 100nm further into the IR than of N3. The photocurrent onset is close to 920nm, i.e. near the optimal threshold for single junction converters. Recently there is a credible challenger identified to the “black dye” (tri(isothiocyanate)-2,2',2''-terpyridyl-4,4'4''-tricarboxylate)Ru ( II ).

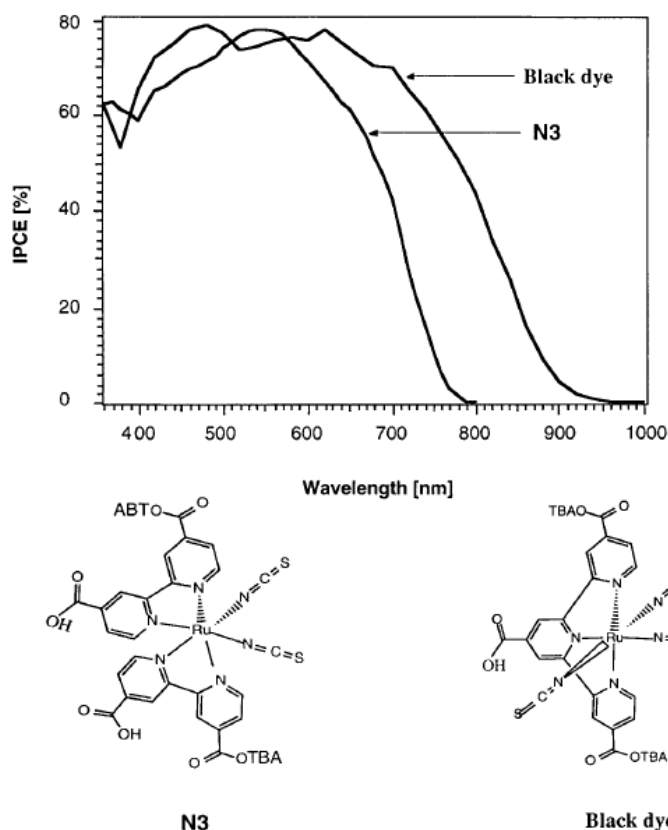


Fig. 2-3 Spectral response curve of the photocurrent for the DSSC sensitized by N3 and the black dye. The chemical structure of N3 dye and black dye. [17]

Lately several studies showed up by modifying the function groups to improve excitation lifetime and increase the open circuit voltage of the cell which are called N719, N749 (black dye)...ect. (Fig.2-4). Recent work has focused on the molecular engineering of suitable ruthenium compounds, which are known for their excellent stability. Cis-Di-(thiocyanato)bis(2,2'-bipyridyl-4,4'-dicarboxylate)ruthenium( II ),



coded as N3 or N719 dye depending on whether it contains four or two protons, was found to be an outstanding solar light absorber and charge-transfer sensitizer. Fig. 2-5 shows the structures of three ruthenium complexes with different colors that have been widely employed as sensitizers for the DSSC. This feature can be applied to design multicolor DSSC in art and architecture.

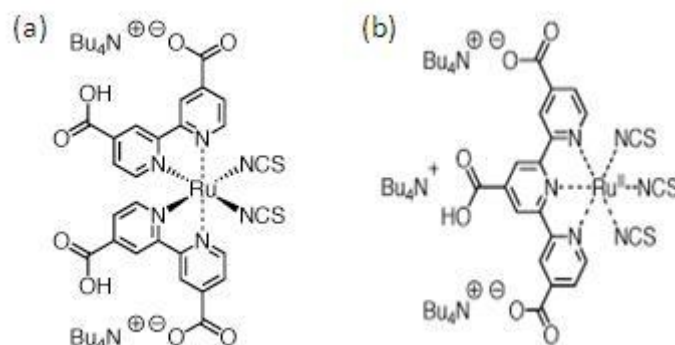


Fig. 2-4 The chemical structure of N719 dye and N749 (black dye). [37]

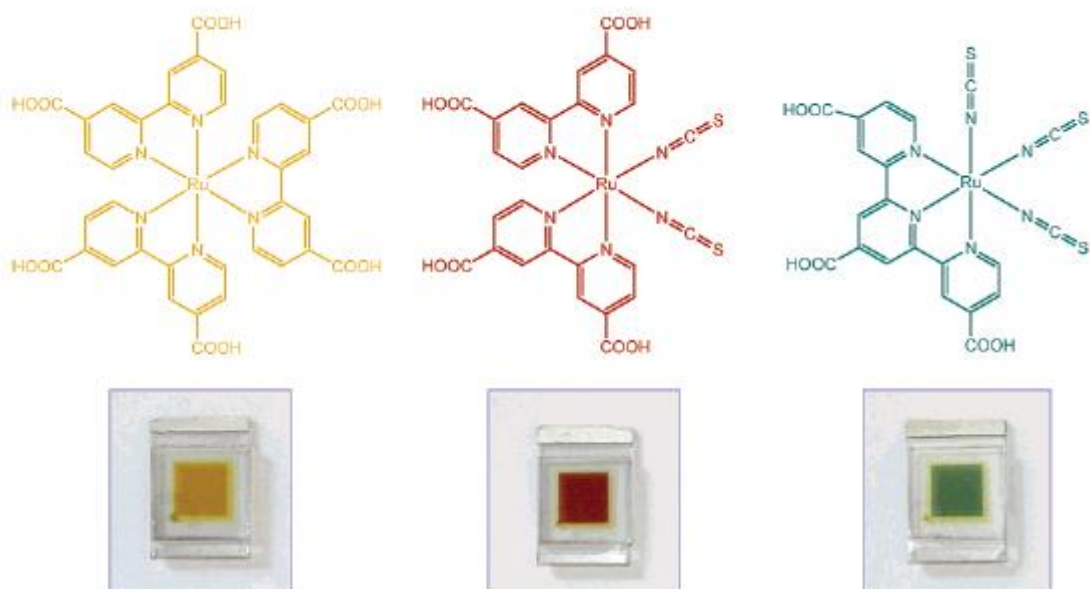


Fig. 2-5 Structure of the ruthenium sensitizers RuL<sub>3</sub> (yellow) *cis*-RuL<sub>2</sub>(NCS)<sub>2</sub> (red) and RuL(NCS)<sub>3</sub> (green) where L) 2,2'-bipyridyl-4,4'-dicarboxylic acid and L) 2,2',2''-terpyridyl-4,4',4''-tricarboxylic acid. The lower part of the picture shows nanocrystalline TiO<sub>2</sub> films loaded with a monolayer of the respective sensitizer. [38]

Another important issue being raised up lately is the dye adsorption process, in which the sintered TiO<sub>2</sub> electrode is immersed into a dye solution, usually 2×10<sup>-4</sup>M in solvent traditionally. The dye adsorption should be done immediately after high temperature sintered process for TiO<sub>2</sub> electrode for not letting water content in the pores of electrode react with the exciting dye molecules and affects the long-term stability. In practice, we keep the photoelectrode in anhydrous condition before and after dye adsorption. The overall dye adsorption process should be stored in a moisture-free environment.

#### **2.2-4 Electrolyte**

Electrolyte systems consist of redox couple and solvent, which works as reductant providing electrons to redox the oxidized dye molecules at photoelectrode and as oxidant receiving from counter electrode.

##### Redox Couples

Requirements and properties of redox couple in electrolyte should be defined:

1. Redox potential

The redox couple reversible potential has to be equal to the negative of dye reversible potential. The more negative the potential, the large the thermodynamic driving force for the dye regeneration. However the potential request should make the balance between the driving and the open circuit potential hence the cell performance in order to avoid unnecessary loss of usable energy.

2. High solubility

To make sure sufficient supply of the redox mediator and to minimize the possibility of diffusion-limited situations, an adequate concentration of redox couple is needed. Because diffusion-limited would result in an undesirable lifetime of the oxidized dye and consequently would increase the possibility of

dye decomposition. Concentration are commonly used at 0.1-0.5M

3. High diffusion coefficient

A high diffusion coefficient is needed because the mass transport of the redox couple in a solar cell (through solution and TiO<sub>2</sub> network) occurs solely by diffusion.

4. No significant spectral characteristics in the visible region

In order to prevent the situation of less light being available for the light-to-electricity conversion and thus low energy conversion, the redox couples should not able to have absorbance in the visible light region.

5. High stability of both the reduced and oxidized forms of couple

For efficient redox “shuttling” in solar cells, both the oxidized and reduced forms of the couple need to be present in solution and both forms must have high stability. In the case of iodide/triiodide system, the reduce form is in excess. [39, 40]

6. Highly reversible couple

The oxidation of the reduce form and reduction of the oxidized form of the redox couple must be electrochemically and chemically reversible to ensure the fast electron transfer and avoid unwanted side reactions.

7. Chemically inert system

The components of the redox couple system must be chemically inert to avoid the side reaction, e.g., no chemical reactivity with TiO<sub>2</sub>, no surface activity, ect.

Based on the requirements listed above, many redox couples have been tested for DSSC systems. Now the I<sup>-</sup>/I<sub>3</sub><sup>-</sup> redox couple still remains the best choice because of its kinetics and suitable redox potential for TiO<sub>2</sub> electrode.

In practical use, the redox couple is prepared by dissolving I<sub>2</sub> and some iodine

salt such as KI, LiI, alkyl methylimidazolium iodide, ect. to form  $I^-/I_3^-$  couple. The triiodide would form instantaneously when iodide is added into iodide via this equation:



Ionic liquid utilizing iodide as anion like DMPII (diemethyl-propyldazium iodide) has also been introduced to be iodide source in DSSC systems. It is believed that those “liquid-like” salts have higher dissociation rate than tradition iodide salt.

### Solvents used for electrolyte

Some criteria are made for a suitable solvent for liquid-type electrolytes as below:

1. The solvents must be liquid and have low volatility at the operation temperature (usually 40-80°C) to avoid freezing or expansion of the electrolyte which would damage the whole cells.
2. They have low viscosity for rapid diffusion of carriers.
3. The chosen redox couple should have high dielectric constant to promote dissolution in solvent.
4. The solvent should not make desorption or dissolution of sensitized dye.
5. The solvent should not decompose under illumination or after long time use.
6. The solvent should better be low cost for large scale production, and have low toxicity.

Typical liquid solvents are acetonitrile (ACN) [41], methoxyacetonitrile, 3-methoxypropionitrile (3-MPN), ethylene carbonate (EC) [42], propylene carbonate[37], ect. and their mixture[43-46]. ACN has performed the best among these solvents, but it is still unwelcoming due to two reasons: (1) highly volatile with low boiling point (82°C) and (2) it is a carcinogenic chemical.

There are also new conceptions for the electrolyte of DSSC: Quasi-solid state polymer electrolyte, using ionic liquid as solvent for electrolytes containing an  $I^-/I_3^-$  redox couple.[47] The request for long-operation stability of DSSC is a driving force of to substitute liquid electrolyte by solid or quasi-solid state electrolyte.[48-52] However, the mass transport of the triiodide has been considered as a limiting factor for ionic liquids due to their low diffusion coefficient and lower concentration in these electrolytes versus iodide. A high concentration of redox couple is needed to achieve a domination of the exchange-reaction based fast charge transport process between  $I^-$  and  $I_3^-$  in viscous electrolytes. On the other hand, the absorption in visible light by  $I^-$  competes with the absorption of the dye and high concentration of  $I^-$  promotes the back electron transfer from conduction band of the photoanode to the triiodide[53].

#### 2.2-5 Counter electrode

The reaction on counter electrode is triiodide reduction:



This reaction plays an important role in the overall DSSC system because it is responsible for the regeneration of oxidized dye molecules. The conversion efficiency of DSSC might be lowered if the speed of dye regeneration is lower than the dye oxidation by photo injection.

Since the ITO or FTO shows slow kinetics of triiodide reduction in organic solvents [54 55], catalytic material is coated in order to accelerate the reduction reaction. Platinum (Pt) has been almost exclusively as the catalytic material. However, different methods preparing thin Pt film lead to different efficiency and cost. Fang *et al.* used sputtered Pt layer and they found out that the sputtered Pt layers on different type of substrates (steel sheet, nickel sheet, polyester film, and conducting plastic film) have slightly different cell efficiencies in comparison with that based on a conducting

glass. [56] In recent reports, Kim *et al.* have demonstrated the preparation of a new counter electrode consisting of Pt nanosized phase in NiO or TiO<sub>2</sub> porous phase using a RF co-sputtering system. They indicated that by applying Pt in a metal oxide biphasic electrode, the short circuit current density and cell efficiency were increased due to the increased active surface area of the nanosized Pt.

Nonetheless, sputtering system is not proper for mass production considering the cost and the environment request of ultra-high vacuum. Papageorgiou *et al.* [57] developed a method called “thermal cluster platinum catalyst” (TCP). Counter electrode made by this method has low Pt loading (around 2-10g/cm<sup>3</sup>), superior kinetic performance, and mechanical stability comparing with other deposition methods like sputtering, spin coating, thermal [5, 58], and electrochemical deposition.

Wei *et al.* [59, 60] developed a simple technique called “two-step dip coating” for preparing a Pt nanoclusters counter electrode for DSSC system. With an appropriate surface conditioner, the adhesion of PVP-capped Pt nanoclusters on ITO glass becomes satisfactory. Electrodes employing this method exhibit not only ultra low Pt usage but also good catalytic performance.

There are still other materials used for counter electrode, such as conducting polymer [61, 62], nanocarbon [63], carbon black [64, 65] and carbon nanotubes [66], some of them even use polymer-catalyst composites [67-69]. These new material used as counter electrode usually requires porous film on the substrate to obtain acceptable catalytic reduction efficiency.

## **2.2-6 Sealant and Spacer**

Sealing is a very important process in DSSC system to avoid the humid environment and to prevent the decomposition of dye molecules. The thickness of spacer is also having dilemma between making lower IR drop and the risk of short

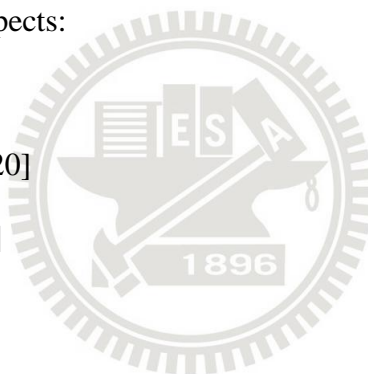
circuit.

Surlyn, a thermoplastic resin which has good toughness, becomes a good sealant used in DSSC. It is inert to electrolyte and shows great tightness. However, there are still other types of resin which also used in DSSC system, and optimal one is not decided.

### 2.2-7 Post-treatment/Pretreatments/Underlayer

Recent paper [70] revealed that a post-treatment of the  $\text{TiO}_2$  film can efficiently improve the performance of DSSC based on the fact that an extra layer of  $\text{TiO}_2$  is grown onto the  $\text{TiO}_2$  nanoparticles constituting the film. There are many hypotheses concerning the following aspects:

- (1) Surface area[20]
- (2) Electron transport[20]
- (3) Light scattering[71]
- (4)  $\text{TiO}_2$  purity[22]
- (5) Dye anchoring[72]



These post-treatments have been carried out by  $\text{TiCl}_3$  electrodeposition, Ti-isopropoxide and, the best, titanium tetrachloride ( $\text{TiCl}_4$ ) post-treatment [70]. The effect of these post-treatment is believed to increase the dye loading making more efficient photon-current conversion which affect the short circuit current density ( $J_{\text{SC}}$ ), and the current conversion efficiency (IPCE). It is also important to note that the  $\text{TiCl}_4$  treatment would not be beneficial if a given  $\text{TiO}_2$  nanoparticle film is already at the correct potential to reach the maximum efficiency of the electron injection, which depends on the history and source of  $\text{TiO}_2$  to be made.

In addition, another report indicates that the  $\text{TiCl}_4$  pretreatment to ITO or FTO can certainly enhances the suppression of dark current leading an increase in  $V_{\text{OC}}$  and

enlarge the surface area of the mesoscopic film leading the improvement of  $J_{SC}$  [73].

Xia *et al.* also present a new FTO/ $TiO_x$ /mesoscopic  $TiO_2$  electrode which can be applied to be the blocking layer of DSSC [74]. According to their study, the blocking layer improved reduction of the electron loss at the FTO/mesoscopic  $TiO_2$  and FTO/electrolyte interface by a  $TiO_2$  compact layer between the FTO and mesoscopic  $TiO_2$  layer which made by RF sputtering system. This is also another discovery finding out a layer made by  $TiO_2$  can improve the total performance of DSSC due to various functions.





## 2.3 TiO<sub>2</sub> morphology control

Mesoporous nanocrystalline TiO<sub>2</sub> films provide large surface area for dye adsorption, electrical connection with the redox electrolyte, electron diffusion and transportation. As the pore size and porosity of the TiO<sub>2</sub> film increases, the diffusion of electrolyte becomes easier, but the effective surface area decrease and the amount of dye adsorb less. Therefore, the morphology of the TiO<sub>2</sub> film plays a very important role in the high efficiency DSSC. There is a precise balance between pore size, porosity, effective surface area and thickness of TiO<sub>2</sub> film to achieve optimum DSSC performance. There are many different methods to modify the morphology of TiO<sub>2</sub> films are reviewed below.

### 2.3-1 Different TiO<sub>2</sub> Particle Size

Mixing different size of TiO<sub>2</sub> particles can control the TiO<sub>2</sub> film morphology easily. Small size TiO<sub>2</sub> particles have high surface area for dye adsorption, and large size TiO<sub>2</sub> particles can contribute larger pore for electrolyte diffusion. Thus, mixing both large and small size of TiO<sub>2</sub> can optimize the TiO<sub>2</sub> film to reach higher photocurrent.

In the research bring up by T. Miyasaka *et al.* [75] mixing different size of TiO<sub>2</sub> particles can increase almost 50% of the cell efficiency. In their study, the best cell efficiency increase to 4.5% if the TiO<sub>2</sub> average particle size is 60nm. The efficiency increase not only because there were good electrolyte diffusion and high surface area for dye adsorption, but large size TiO<sub>2</sub> particle in the TiO<sub>2</sub> film could act as light-scattering particles to efficient the light absorption.

The more specific study were reported by S. H. Kang *et al.* [76] They mixed large size (70 to 100nm) TiO<sub>2</sub> particles into TiO<sub>2</sub> film, and changed the mixing ratio to reach the highest conversion efficiency of DSSC (4.75%). The TiO<sub>2</sub> film with 10wt%

light scattering particles (large size  $\text{TiO}_2$  particles) showed enhanced performance (28%), compared with standard nanocrystalline  $\text{TiO}_2$  films.

### 2.3-2 Multi-Layer of $\text{TiO}_2$ Film

Reaches brought up that using multi-layer instead of single-layer for  $\text{TiO}_2$  film can increase the cell conversion efficiency. The compact  $\text{TiO}_2$  layer was added between original  $\text{TiO}_2$  film and TCO glass called blocking layer. [77, 78] This blocking layer is usually made by dense  $\text{TiO}_2$  particles or thin  $\text{TiO}_2$  block film, which can reduce electron recombination at TCO glass and electrolyte interface efficiently. Also, the blocking layer can improve the adherence of  $\text{TiO}_2$  to TCO glass surface; provide larger contact area for electron transfer from  $\text{TiO}_2$  film to TCO glass. Blocking layer can increase both short circuit current density and open current voltage to reach higher conversion efficiency. In the reports, the addition of blocking layer increased almost 30% of cell efficiency.

One more layer on the original  $\text{TiO}_2$  layer with larger  $\text{TiO}_2$  particle size is called light-scattering layer. [79] With this addition layer, light-scattering layer on the  $\text{TiO}_2$  film, the photocurrent of DSSC device was increased nearly 40%, compared with the device without the light-scattering layer. It is because the scattering property of this  $\text{TiO}_2$  film had the light captured inside the device. In the study of B.F. Huang *et al.* [80], larger particle size can have better light scattering property. They achieved a high efficiency 8.84% with light scattering layer particle radius 600-800nm.

Combine all these layers to form a multi-layer  $\text{TiO}_2$  film would be the best for DSSCs. L. Hu *et al.* [81] produce a three layer  $\text{TiO}_2$  photoelectrode, included layers of small particle size film, large particle size film and light-scattering particle film for DSSC. To decrease the contact interface between TCO glass and electrolyte and increase the electron transfer from  $\text{TiO}_2$  to electrode, smaller size particles, lower

porosity and more compact layer should be innermost layer. To efficient the diffusion of electrolyte to regenerate dye, the larger size  $\text{TiO}_2$  particle should deposit next and the light scattering layer should be on the most top of the  $\text{TiO}_2$  film.

### 2.3-3 $\text{TiO}_2$ Nanotube

Recently,  $\text{TiO}_2$  nanotube is also introduced to DSSCs using in  $\text{TiO}_2$  layers. The  $\text{TiO}_2$  can be produce by electrophoretic deposition (EPD) [82], template replica process [83-87], sol-gel method [88], hydrothermal method and anode oxidization ect. Changing the charge transport to one dimension in  $\text{TiO}_2$  nanotube can reduce the power loss when charge transfer between  $\text{TiO}_2$  particles.

In the study of L. Zhoa *et al.* [83], high order  $\text{TiO}_2$  nanotube was made by electrophoretic deposition and introduce to DSSC. The DSSCs with  $\text{TiO}_2$  nanotube shows higher efficiency than the cells made from commercial-grade Degussa P25  $\text{TiO}_2$  nanoparticles. One dimension structure of ordered  $\text{TiO}_2$  nanotube films provided a high rate electron transfer along the  $\text{TiO}_2$  nanotube and expected to enhance the diffusion of electrolyte in DSSCs.

Lee *et al.* [89] mixed  $\text{TiO}_2$  nanotube and  $\text{TiO}_2$  nanoparticle for  $\text{TiO}_2$  films for DSSCs with a new type sensitizer (FL).  $\text{TiO}_2$  nanoparticles have high surface area for dye adsorption, and  $\text{TiO}_2$  nanotube have higher electron transport rate. By mixing both kinds of  $\text{TiO}_2$ , better  $\text{TiO}_2$  films were made and introduced to DSSCs. In their study, the  $\text{TiO}_2$  film containing 5wt%  $\text{TiO}_2$  nanotube has respectable cell conversion efficiency 7.8%.

### 2.3-4 Special $\text{TiO}_2$ Nanostructure

There are many special  $\text{TiO}_2$  nanostructures were introduced to DSSC's  $\text{TiO}_2$  film for higher DSSC conversion efficiency. Hollow  $\text{TiO}_2$  sphere is one of these

special TiO<sub>2</sub> nanostructures. J. Yu *et al.* [90] synthesized the hollow TiO<sub>2</sub> sphere by a chemical introduce self-transformation strategy using urea as a base catalyst, whose walls are composed of anatase nanocrystals and exhibit hierarchical porosity. J. H. Park *et al.* [91] used paste method with polymer templates also can synthesize hollow TiO<sub>2</sub> sphere successfully. TiO<sub>2</sub> hollow structured materials not only have low density, high specific surface area and hierarchical porous structure, but also exhibit high light-collection efficiency and fast motion of charge carriers. The DSSC with TiO<sub>2</sub> hollow structured film has better cell efficiency than DSSC with TiO<sub>2</sub> film constructed by noaparticle.

Y. J. Kim *et al.* [92] provided another kind of TiO<sub>2</sub> spheres for DSSCs. The nanoporous TiO<sub>2</sub> sphere with a diameter about 250nm is prepared by a specially designed solvothermal treatment. These TiO<sub>2</sub> spheres consisted of 12-13nm TiO<sub>2</sub> grains with ultrahigh surface area and well-developed nanopore structure. The large external pores formed among the spheres will work as a “highway” for electrolyte diffusion through thick TiO<sub>2</sub> film and minimized the diffusion distance of electrolyte in TiO<sub>2</sub> nanograins to 125nm (half of the sphere). The TiO<sub>2</sub> sphere structure also offer a considerable scattering effect in long-wavelength region. Because of these advantages, the DSSC efficiency reached 8.44%, with 15% increase.

Cauliflower like TiO<sub>2</sub> spheres was synthesized by L. Tang *et al.* [105], and using as scattering center in TiO<sub>2</sub> film of DSSC. Cauliflower-like TiO<sub>2</sub> rough spheres with size about 200nm greatly enhanced the light harvesting efficiency and energy conversion efficiency of DSSC due to their high light scattering effect and large surface area compare to smooth spheres. By adding 25wt% of cauliflower like TiO<sub>2</sub> spheres into TiO<sub>2</sub> film, the conversion efficiency achieved 7.36%.

### 2.3-5 Dispersive Polymer Addition

A more easy way to control the morphology of TiO<sub>2</sub> film is adding dispersive polymer into TiO<sub>2</sub> paste before film coating, which can change the film surface area, pore size and porosity. Poly(ethylene glycol) (PEG) [94,95], poly(methylmethacrylate) (PMMA) [96, 97] and polystyrene (PS) [14] are three common polymers used in TiO<sub>2</sub> coating paste as addition.

Control the dispersive polymer loading in the TiO<sub>2</sub> paste can easily change the porosity of the TiO<sub>2</sub> film, and increase the DSSC conversion efficiency. But there are an optimized loading for these polymers. Overloading might cause damage of TiO<sub>2</sub> films and decrease the cell conversion efficiency. Suitable addition of dispersive polymer improve the cell efficiency because increase the porosity of TiO<sub>2</sub> electrode can facilitate the electrolyte to penetrating more deeply into dye-sensitized TiO<sub>2</sub> film, and speed up the dye regeneration especially in gel-type electrolyte case. The pore inside TiO<sub>2</sub> film also can act as light-scattering center for investing higher photocurrent.[98, 99]

In the study of Y. Saito *et al.* [12], the PEG addition was not only affecting the porosity but also the roughness factor (*rf*) of TiO<sub>2</sub> film. Increase of PEG addition the porosity increase and the roughness factor decrease. Smaller porosity would prevent effective penetration and adsorption of dye molecules on TiO<sub>2</sub> film and slow the electrolyte diffusion. Higher roughness factor of TiO<sub>2</sub> meant there was longer distance from the dye to the TCO glass electrode and also increased electron recombination. There was an optimized loading amount of PEG (10%) which achieved 5.65% cell conversion efficiency.

Adding different molecular weight of PEG into TiO<sub>2</sub> paste would change the surface area and pore size of TiO<sub>2</sub> film. [106] Larger molecular weight PEG contributed larger pore size but smaller surface, and smaller molecular weight PEG

was in the contrast. Larger pores may allow more redox species diffusing inside the pore, which can reduce the resistance at  $\text{TiO}_2$ /dye/electrolyte interface. However, larger surface can make more dye adsorption to increase the photocurrent. In this study, they combine these two different  $\text{TiO}_2$  films to become a multi-layer  $\text{TiO}_2$  electrode which have high surface and larger pore size; and reach 9.04% DSSC conversion efficiency.



## 2.4 Instrument Methodologies

### 2.4-1 Brunauer–Emmett–Teller

Brunauer–Emmett–Teller (BET) theory aims to explain the physical adsorption of gas molecules on a solid surface and serves as the basis for an important analysis technique for the measurement of the specific surface area of a material. [98]

The concept of the theory is an extension of the Langmuir theory, which is a theory for monolayer molecular adsorption, to multilayer adsorption with the following hypotheses: (a) gas molecules physically adsorb on a solid in layers infinitely; (b) there is no interaction between each adsorption layer; and (c) the Langmuir theory can be applied to each layer. The resulting BET equation is expressed by (2-15):

$$\frac{1}{n\left[\left(\frac{P}{P_0}\right) - 1\right]} = \frac{c - 1}{n_m} \left(\frac{P}{P_0}\right) + \frac{1}{n_m c} \quad (2-15)$$

$P$  and  $P_0$  are the equilibrium and the saturation pressure of adsorbates at the temperature of adsorption,  $n$  is the adsorbed gas quantity (for example, in volume units), and  $n_m$  is the monolayer adsorbed gas quantity.  $c$  is the BET constant, which is expressed by (2-16):

$$c = \exp\left(\frac{E_1 - E_L}{RT}\right) \quad (2-16)$$

$E_1$  is the heat of adsorption for the first layer, and  $E_L$  is that for the second and higher layers and is equal to the heat of liquefaction.

Equation (2-15) is an adsorption isotherm and can be plotted as a straight line with  $1/n[(P/P_0) - 1]$  on the y-axis and  $\phi = P/P_0$  on the x-axis according to experimental results. This plot is called a BET plot. The linear relationship of this equation is maintained only in the range of  $0.05 < P/P_0 < 0.35$ . The value of the slope

(A) and the y-intercept (I) of the line are used to calculate the monolayer adsorbed gas quantity  $n_m$  and the BET constant  $c$ . The following equations can be used:

$$n_m = \frac{1}{A + I} \quad (2-17)$$

$$c = 1 + \frac{A}{I} \quad (2-18)$$

The BET method is widely used in surface science for the calculation of surface areas of solids by physical adsorption of gas molecules. A total surface area  $S_{total}$  and a specific surface area  $S_{BET}$  are evaluated by the following equations:

$$S_{total} = \frac{(n_m N s)}{V} \quad (2-19)$$

$$S_{BET} = \frac{S_{total}}{a} \quad (2-20)$$

where  $n_m$  is in units of volume which are also the units of the molar volume of the adsorbent gas,  $N$  is the Avogadro's number,  $s$  is the adsorption cross section of the adsorbing species,  $V$  is the molar volume of adsorbent gas and  $a$  is the mass of adsorbent (g)

### Average Pore Diameter

There are two useful equations for estimating the average pore diameter, the first one is

$$d = 4V_L/A$$

where  $d$  is the average pore diameter,  $V_L$  is the volume of adsorbate necessary to fill pores computed as normal liquid which can be the pore volume in BET analysis and  $A$  the surface area. And another one is



$$d = 6.56 \frac{M}{\rho a} \frac{1}{1 - j}$$

where  $d$  is the average pore diameter,  $M$  and  $\rho$  the molecular weight and density of adsorbate, respectively, and  $a$  the cross-sectional area of the adsorbate molecule.

By these two equations, the average pore diameter can be calculated by data we get from BET analysis. [99]

### **Pore Size Distribution**

Numbers of method were developed for the pore size distribution analysis. Since the development of the pore size distribution calculation method based on the so-called Non Local Density Functional Theory (NLDFT), the methods based on this approach became widely used for the characterization of pore structure of activated carbons and other porous materials.

Detailed description of the DFT approach to the pore size analysis had been studied. Briefly, the evaluation of pore size distribution is based on the theoretical isotherms calculated for individual pores of a given adsorbate-adsorbent system. These isotherms are generated using the NLDFT where the fundamental molecular parameters characterizing the gas-gas and gas-solid interactions of the adsorption system are utilized. Mathematical procedure used to calculate pore size distribution can be described as fitting a combination of the theoretical isotherms to the experimental data. The obtained pore size distribution represents volumetric contributions of pores with different sizes whose theoretical isotherms best fit the experimental data. [100]

### **2.4-2 Electrochemical Impedance Spectroscopy (EIS)**

Electrochemical Impedance Spectroscopy also known as Dielectric Spectroscopy

measures the dielectric properties of a medium as a function of frequency. It is also an experimental method of characterizing electrochemical systems. This technique measures the impedance of a system over a range of frequencies, and therefore the frequency response of the system, including the energy storage and dissipation properties, is revealed. Often, data obtained by EIS is expressed graphically in a Bode plot or a Nyquist plot.

Impedance is the opposition to the flow of alternating current (AC) in a complex system. A passive complex electrical system comprises both energy dissipater (resistor) and energy storage (capacitor) elements. This technique has grown tremendously in stature over the past few years and is now being widely employed in a wide variety of scientific fields such as fuel cell testing, biomolecular interaction, and microstructural characterization. [101-104]

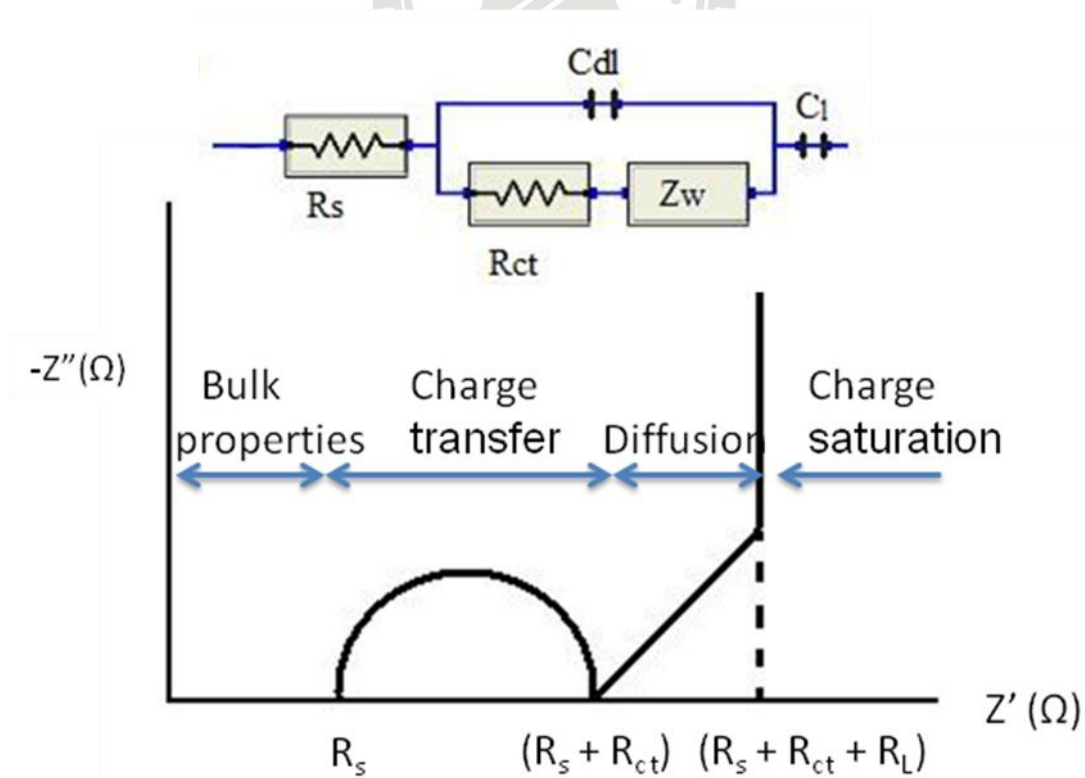


Fig. 2-6 An Ideal Nyquist Plot

Often, EIS reveals information about the reaction mechanism of an electrochemical process: different reaction steps will dominate at certain frequencies, and the frequency response shown by EIS can help identify the rate limiting step.

Fig. 2-6 is an ideal Nyquist Plot, and there are three parts in this plot, high frequency kinetic control regime, mid-frequency diffusion control regime and low frequency charge saturation regime. The kinetic control regime shows a semi-circle impedance spectrum, which is determined by charge transfer ability when redox reaction. The diffusion control regime shows a  $45^\circ$  line, which is affected by charge diffusion in electrodes. The charge saturation regime shows a vertical line, which is affected by electrode thickness and saturated charge diffusion.

By the EIS can come out with an equivalent circuit by simulation. And from this equivalent circuit, the further information of electrochemical properties can be studied. For DSSCs, the equivalent circuit is usually the same. The equivalent circuit of DSSCs with liquid type electrolyte shows below.

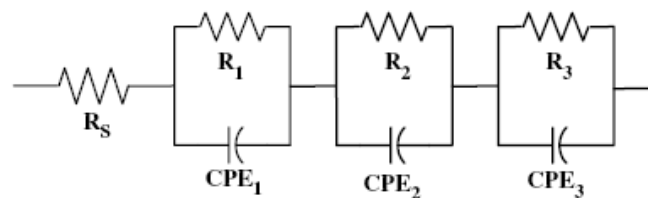


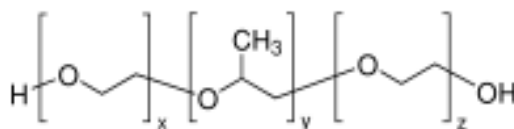
Fig. 2-7 The equivalent circuit for the DSSCs with liquid type electrolyte

## Chapter 3 Experimental Section

### 3.1 Materials

#### Materials for TiO<sub>2</sub> paste

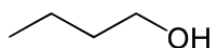
1. Titanium dioxide Degussa P25 powder
2. Poly(ethylene glycol)-block- Poly(propylene glycol)-block- Poly(ethylene glycol) (P123) from Aldrich as a binder in TiO<sub>2</sub> paste and the chemical structure is :



3. Polyethylene glycol (PEG) with molecular weight 35,000 and 100,000 from Aldrich as a morphology controller in TiO<sub>2</sub> paste and the chemical structure is:



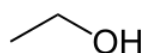
4. N-butanol (C<sub>4</sub>H<sub>9</sub>OH) from ECHO as the solvent for TiO<sub>2</sub> paste:



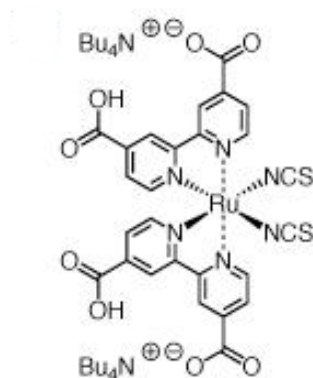
5. Titanium dioxide 100nm nanoparticles from ISK for light-scattering layer

#### Materials for DSSCs

1. Titanium tetrachloride (TiCl<sub>4</sub>) from SHOWA for post-treatment of TiO<sub>2</sub> film
2. Fluorine-doped tin oxide (FTO) conducting glass (8Ω/sq) from Hartford Glass
3. Ethanol (C<sub>2</sub>H<sub>5</sub>OH) from ECHO as a solvent for dye solution and the chemical structure is:

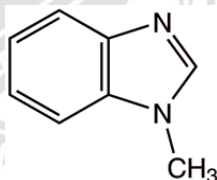


4. Surlyn® (SX1170-60) from SOLARONIX as the spacer and sealing material
5. N719 dye from UniRegion Bio-Tech and the chemical structure is:

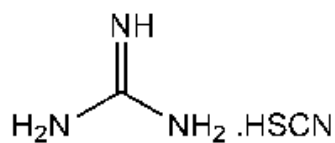


### Materials for electrolyte

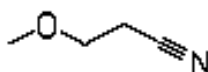
1. Lithium iodide (LiI) from MERCK
2. Iodine (I<sub>2</sub>) from SHOWA
3. 1-methylbenzimidazole from Alfa Aesar and the chemical structure is:



4. Guanidine thiocyanate from Alfa Aesar and the chemical structure is:



5. 1-Methoxypropionitrile from Alfa Aesar as a solvent for the electrolyte and the chemical structure is:



## 3.2 TiO<sub>2</sub> Paste Preparation

### 3.2-1 TiO<sub>2</sub> paste composition

The TiO<sub>2</sub> paste consist of commercial TiO<sub>2</sub> nanoparticles (P25 powder, Degussa), poly(ethylene glycol)-block-Poly(propylene glycol)-block-Poly(ethylene glycol) (P123) as binder, and polyethylene glycol (PEG) as porogen with butanol or water as solvent. In this study, we change the loading amount of PEG and different solution to control the pore morphology of TiO<sub>2</sub> film. The composition of varies TiO<sub>2</sub> pastes are shown below:

Table 3-1 TiO<sub>2</sub> paste composition in butanol solution

	0% PEG	5% PEG	10% PEG	15% PEG	20% PEG
TiO <sub>2</sub> (P25)	0.3g				
P123	0.1g				
PEG (35k or 100k)	0g	0.1g	0.2g	0.4g	0.6g
H <sub>2</sub> O	0.1g				
Butanol	1.2g	1.4g	1.4g	1.6g	1.6g

Table 3-1 shows TiO<sub>2</sub> paste composition in butanol solution. The water addition is for PEG dissolution because PEG is hardly dissolved in butanol. The difference of butanol amount is for adjusting the paste viscosity to control the TiO<sub>2</sub> film thickness at coating process. The PEG loading is set to 0%, 5%, 10%, 15% and 20% with two different molecular weights of PEG, 35,000 and 100,000. Table 3-2 shows TiO<sub>2</sub> paste composition in water solution. TiO<sub>2</sub> pastes with both kinds of PEGs. And the paste of TiO<sub>2</sub> scattering layer was composed of 0.3g 100nm TiO<sub>2</sub> powder and 0.3g P123 in 2.4g n-butanol solvent.

Table 3-2 TiO<sub>2</sub> paste composition in water solution

	TiO <sub>2</sub> (P25)	P123	PEG (35k or 100k)	H <sub>2</sub> O
15% PEG (35k)	0.3g	0.1g	0.4g	1.5g
15% PEG (100k)	0.3g	0.1g	0.4g	1.5g

### 3.2-2 TiO<sub>2</sub> paste mixing process

The uniform TiO<sub>2</sub> paste is important. The TiO<sub>2</sub> nanoparticles might aggregate to form large particles which would lose their high surface area and cause TiO<sub>2</sub> film crack after film coating. The mixing procedures of the paste are:

1. Mixing PEG, P123 and the solution (butanol and water) and ultrasonic disperse to the mixture mixed well.
2. Mixing TiO<sub>2</sub> and the mixture made at first step with stirring stick in the sample bottle.
3. Ultrasonic dispersing for 2 hours through room temperature water to prevent the solvent evaporation.
4. Stirring the sample by stirring or stirrer bar for 10 minutes.
5. Ultrasonic dispersing for 10 hours through room temperature water.
6. Settling for 1 hour but no longer than 2 hours before use.

### 3.3 TiO<sub>2</sub> film Preparation

FTO (fluorine-doped tin oxide) conducting glass ( $8\Omega/\text{sq}$ ) was cleaned by ultrasonic sieving for 20 min. The TiO<sub>2</sub> paste was coated to film on FTO glass by doctor-blade method. The TiO<sub>2</sub> film thickness and active area ( $0.28\text{ cm}^2$ ) was controlled by adhesive tape with thickness 110 nm. After coating, the TiO<sub>2</sub> film was dried at room temperature in the air for one minute and removed the adhesive tape. Then, the TiO<sub>2</sub> anode was sintered at  $400^\circ\text{C}$  for 40 minutes and also for removing the organic loads. Here, we change the PEG burn-out rate which could also control the TiO<sub>2</sub> film morphology. The two different burn-out rates show below:

1. Burn out PEG loading in TiO<sub>2</sub> film directly at  $400^\circ\text{C}$  for 40minutes.
2. The TiO<sub>2</sub> film was baked at  $100^\circ\text{C}$  for 30 minutes and the temperature was raised to  $400^\circ\text{C}$  in 15 minutes then burned out PEG loading and sintered for 40min at  $400^\circ\text{C}$ .

Backing the TiO<sub>2</sub> electrode at  $100^\circ\text{C}$  for 30min could let PEG have time and energy to aggregate and form larger size pores after being burned out. After cooling down, the adhesive tape was applied again to define the same area for the scattering TiO<sub>2</sub> layer coating. The scattering TiO<sub>2</sub> layer was deposited by spin-coating with 600 rpm spin speed for 25 seconds and the TiO<sub>2</sub> anode was also sintered at  $400^\circ\text{C}$  for 30minutes after remove the adhesive tape. Figure 3-1 shows the schematic diagram of coating process.



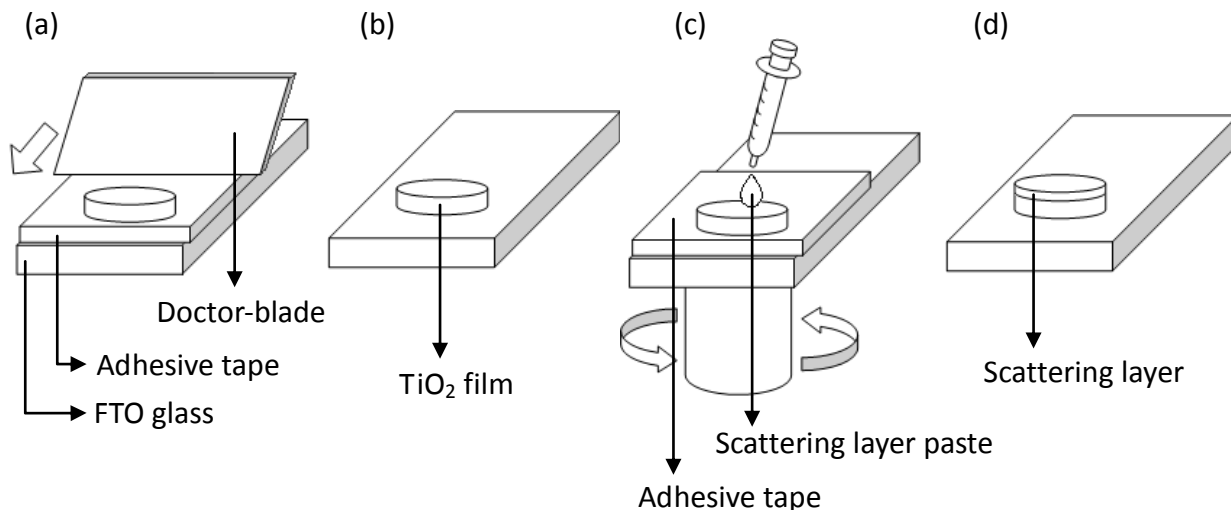


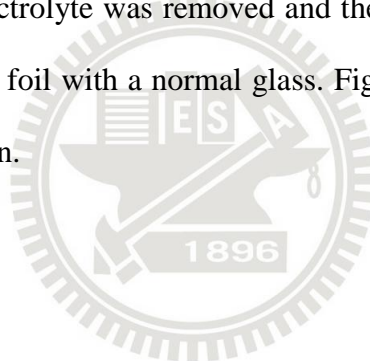
Fig. 3-1 Coating process of the  $\text{TiO}_2$  film. (a) Doctor-blade coating  $\text{TiO}_2$  film. (b)  $\text{TiO}_2$  film sintered at  $400^\circ\text{C}$ . (c) Spin-coating scattering layer. (d)  $\text{TiO}_2$  electrode sintered at  $400^\circ\text{C}$ .

The post-treatment was done by immersing the  $\text{TiO}_2$  anode into the 0.1 M  $\text{TiCl}_4$  water solution for 30 min in ice bath to form a very thin  $\text{TiO}_2$  layer on  $\text{TiO}_2$  particles which can improve the charge transfer between  $\text{TiO}_2$  particles and dye adsorption.[64 93] After  $\text{TiCl}_4$  treatment, the  $\text{TiO}_2$  anode was sintered at  $400^\circ\text{C}$  for one hour to crystallize the  $\text{TiO}_2$  film to anatase phase.

The samples for BET analysis were also coated by doctor-blade method, and sintered by the same process. But the scattering layer and the post-treatment were not done for these samples. The  $\text{TiO}_2$  films was scratched off from the FTO glass, and collected to certain amount for BET analysis.

### 3.4 DSSCs fabrication

The TiO<sub>2</sub> photoanode was immersed in a 3×10<sup>-4</sup>M N719 dye ethanol solution at room temperature for 24 hours for dye adsorption. After sensitized, the TiO<sub>2</sub> photoanode was dip into ethanol to remove extra dye which did not adsorb on the TiO<sub>2</sub> surface. DSSC was fabricated by sealing the dye-sensitized TiO<sub>2</sub> photoanode and Pt-sputtered counter electrode around 100°C with hot melt sealing foil. The hot melt sealing foil was also a 60 μ m spacer. There are two little holes on the Pt-sputtered counter electrode for electrolyte injection. The electrolyte composition was 0.5M LiI, 0.05M I<sub>2</sub>, 0.2M 1-methylbenzimidazole and 0.5M guanidine thiocyanate in 1-Methoxypropionitrile solvent and was injected into the two little holes on the counter electrode. Extra electrolyte was removed and the two little holes were sealed also by the hot melt sealing foil with a normal glass. Figure 3-2 shows the schematic diagram of DSSC fabrication.



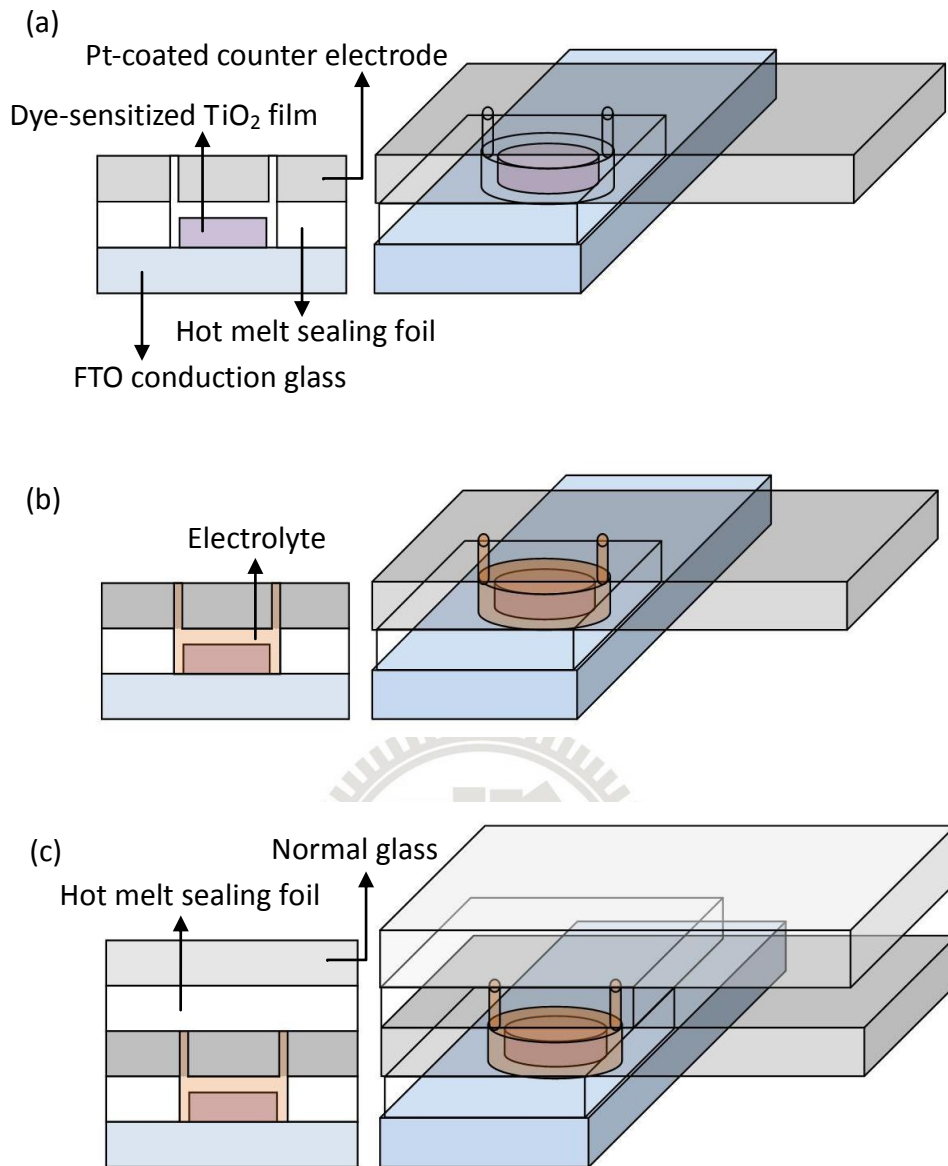


Fig. 3-2 The DSSC fabrication process. (a) Sealing the dye-sensitized photoanode and Pt-coated counter electrode. (b) Electrolyte injection. (c) Sealing the electrolyte injection holes on counter electrode.

## **3.5 Characterization Techniques**

### **3.5-1 Brunauer–Emmett–Teller (BET) Analysis**

The pore size, pore size distribution, porosity and surface area of TiO<sub>2</sub> film was measured by Brunauer–Emmett–Teller (BET) method, using Surface Area and Pore Size Analyzer (NOVA 1000e). The measurement point setting was 0-0.3 P/P<sub>0</sub> 17 points, 0.3-1 P/P<sub>0</sub> 7 points, 1-0 P/P<sub>0</sub> 15 points.

### **3.5-2 Scanning Electron Microscopy (SEM)**

SEM is a powerful microscopy method for close viewing of nanoparticles. The microstructure of TiO<sub>2</sub> films was studied by a scanning electron microscopy (SEM, HITACHI-S2500 JSM-6500F). The TiO<sub>2</sub> film was coated on normal glass for easier SEM sample preparation. The porous TiO<sub>2</sub> film was observed by SEM including nanoparticle TiO<sub>2</sub> film and light-scattering layer. And the film thickness also defined by SEM observation.

### **3.5-3 Uv-Visible Light Spectrum**

The amount of dye adsorption was determined by desorbing the dye from TiO<sub>2</sub> film surface into 5mM NaOH aqueous solution and measuring its light absorbance by Uv- visible light spectrometer. The dye adsorption of TiO<sub>2</sub> film could be calculated by comparing the absorption intensity of dye desorbed NaOH solutions and a reference NaOH solution, and a reference dye solution with concentration  $8 \times 10^{-5} \text{M}$  was used for calculation.

### **3-5-4 Photocurrent Examination**

The AM1.5 solar simulator (Newport 3A) was used as the light source, and the incident light spectrum was AM1.5, 1 sun ( $100\text{mW}/\text{cm}^2$ ) calibrated with standard Si solar cell (ORIEL). The I-V curve was recorded with Keithley by scanning DSSC from -0.2V to 0.8V, and the photoelectrochemical characterizations of DSSCs were carried out by computer calculation with the active area  $0.28\text{cm}^2$ .

### **3-5-5 Electrochemical Impedance Spectroscopy (EIS)**

The impedances between the interfaces inside DSSCs were measured by electrochemical impedance spectroscopy (EIS) and presented in the form of the Nyquist plots. The EIS measurements were performed using AC impedance (PGSTAT100 AUTOLAB, Netherlands) over the frequency range from 0.01 to  $10^6$  Hz with amplitudes 10mV. The results from EIS were then compared and discussed with the efficiency results to provide a more specific explanation of the influence of the changes of  $\text{TiO}_2$  films.

### 3.6 Experimental Flow

The well mixed TiO<sub>2</sub> paste was prepared with different solvents and then coating into films by doctor-blade method followed with sintering and PEG burn out process. The SEM image was taken for thickness pore morphology observation of TiO<sub>2</sub> film. The TiO<sub>2</sub> films were scratched down from the FTO glass for the BET measurement. And the pore size, porosity and surface area were analyzed. The TiO<sub>2</sub> electrode was immersed into the dye solution for dye adsorption, then the dye desorbed into NaOH water solution for Uv-visible measurement. By Uv-visible spectrum, the dye adsorption amount could quantify after calculation. The TiO<sub>2</sub> electrodes with light-scattering layer after TiCl<sub>4</sub> post-treatment were dye-sensitized and fabricated into DSSCs for efficiency measurement and EIS analysis. The relationship between pore morphology and DSSC performance would discuss.

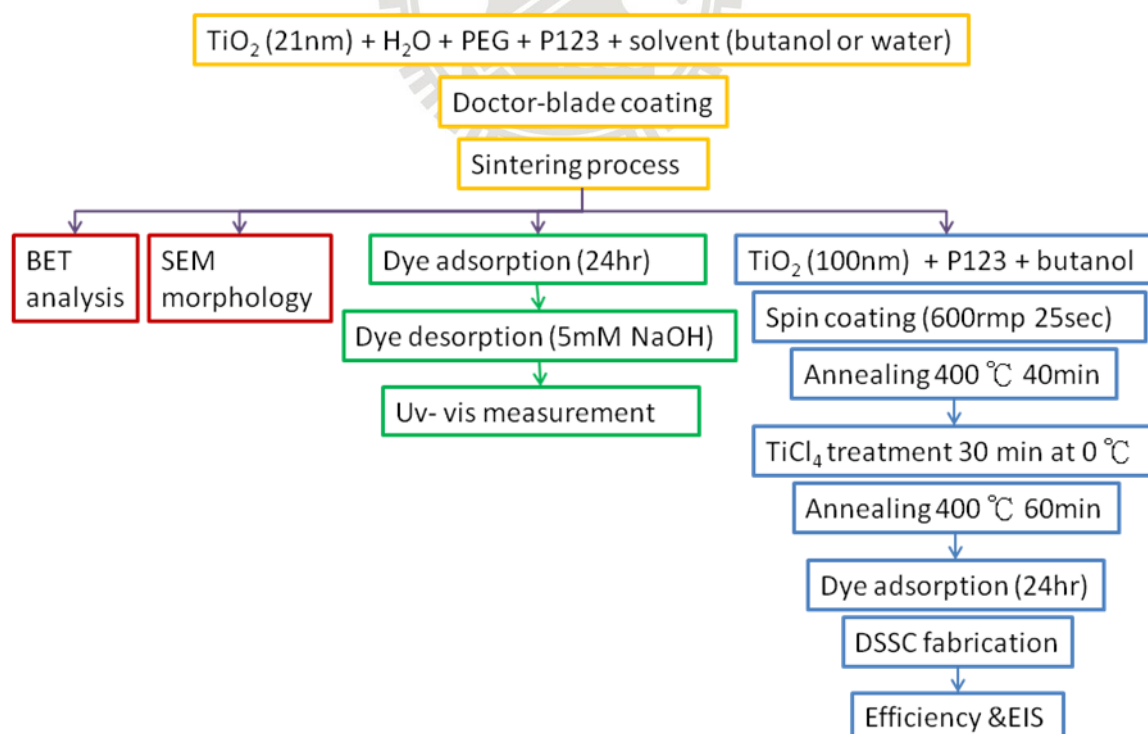


Fig. 3-3 Experiment Design chart

## Chapter 4 Results and Discussion

### 4.1 Characterization of TiO<sub>2</sub> films

#### 4.1-1 Surface morphology and film thickness of TiO<sub>2</sub> film

Surface morphology and film thickness of TiO<sub>2</sub> films with different PEG loadings are examined by SEM and shown in Fig. 4-1. The large pores (> 100 μm) were not caused by PEG addition, but caused by TiO<sub>2</sub> chip-off process during SEM sample preparation. The SEM image (Fig. 4-1(a)) shows that the structure of TiO<sub>2</sub> film with 5% PEG loading is still dense, indicating that its morphology is not affected much by the PEG addition. In contrast, highly porous nanostructures were observed in the TiO<sub>2</sub> films prepared by pastes with PEG loadings at 10% and 15%, as illustrated by Figs. 4-1(b) and (c). The porosity increased with increasing PEG loading up to 15%. However, the SEM graph of TiO<sub>2</sub> film with 20% PEG loading shows that the structure becomes dense with a smaller porosity. This may be attributed to too many pores within the TiO<sub>2</sub> film at high PEG loading, resulting in film collapse and densification.

Based on SEM measurement, the thicknesses of TiO<sub>2</sub> films with PEG loading at 5%, 10%, and 15% remain approximately the same (~15 μm) as shown in Figs. 4-1(e), (f), and (g), respectively. However, the TiO<sub>2</sub> film thickness is reduced to 12 μm as shown in Fig. 4-1(h) when PEG loading is increased to 20%. This confirms that the TiO<sub>2</sub> structure collapses if PEG loading is ≥20%. As a result, the PEG loading in this study is kept below than 20% to avoid any damage and collapse in the TiO<sub>2</sub> nanostructure.

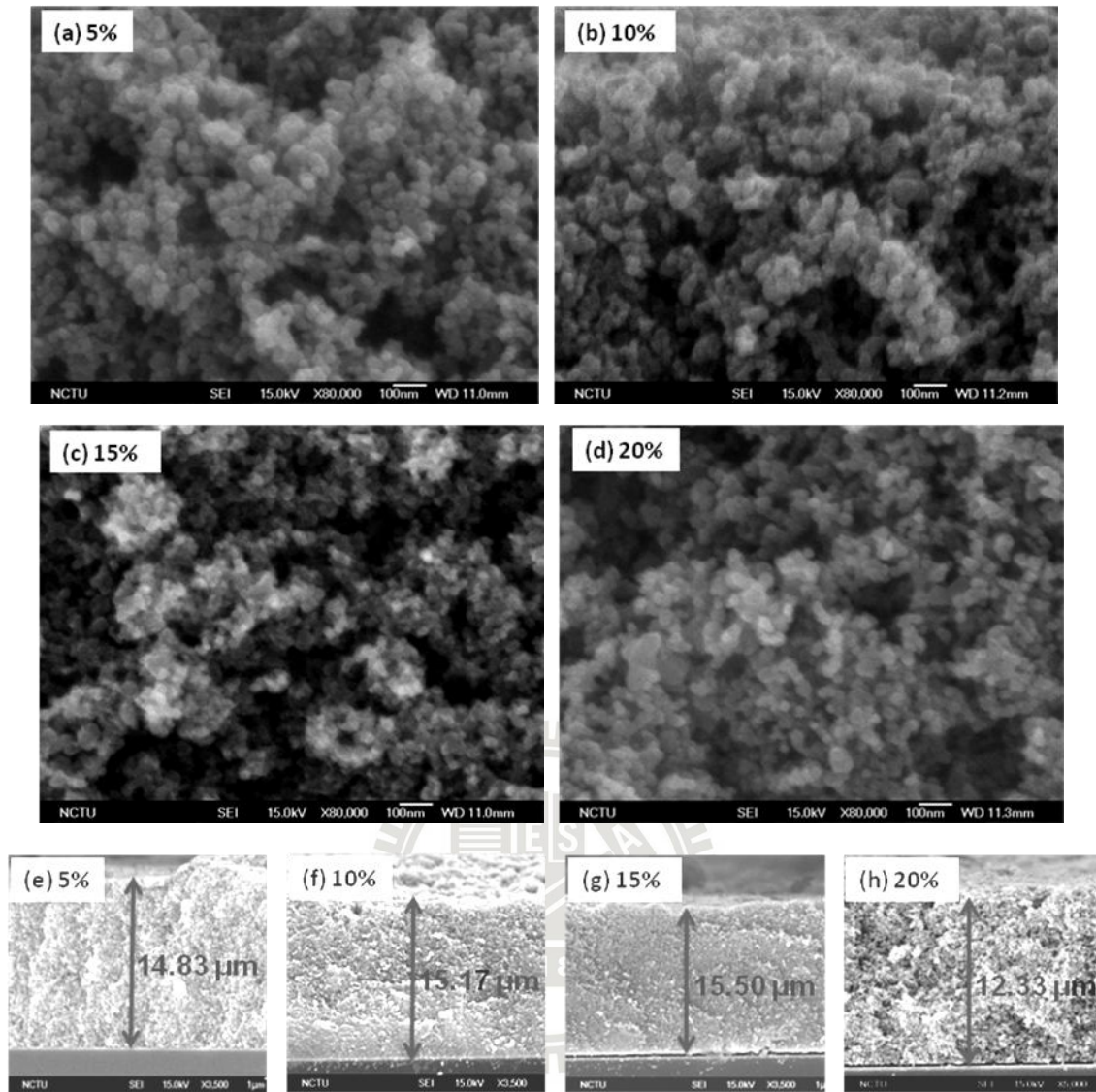


Fig. 4-1 The surface morphology and film thickness of  $\text{TiO}_2$  electrodes prepared at various PEG loadings (5, 10, 15, and 20%) (a)-(d): surface morphology; (e)-(h):  $\text{TiO}_2$  film thickness

Next, the film stacking of  $\text{TiO}_2$  electrode with light-scattering layer is examined. The scattering layer (100 nm  $\text{TiO}_2$  particles) is spin-coated onto the  $\text{TiO}_2$  film consisting of 21 nm  $\text{TiO}_2$  particles. The thickness of the light-scattering layer is about 4  $\mu\text{m}$  and uniform across the sample by SEM measurement, as shown in Fig. 4-2. The uniform particle sizes of  $\text{TiO}_2$  particles and light-scattering particles are also observed by SEM as shown in Fig. 4-2. After the coating of a light-scattering layer, the total  $\text{TiO}_2$  film thickness was about 19-20  $\mu\text{m}$ , which has been previously reported as the



optimized TiO<sub>2</sub> film thickness (20 μm) by Shin *et al.* [94]

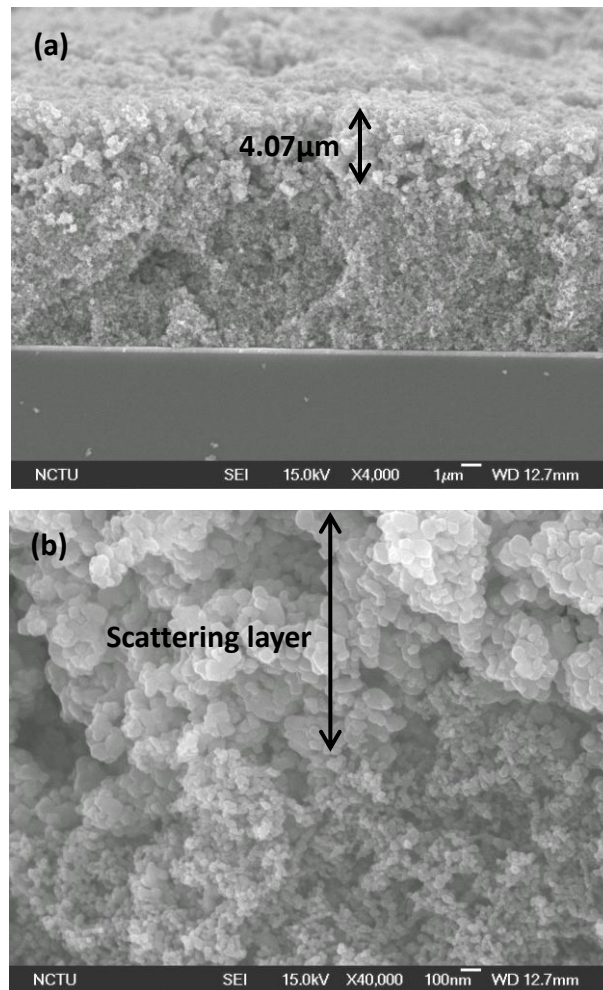


Fig. 4-2 SEM image of (a) scattering layer (100 nm TiO<sub>2</sub> particles) coated on TiO<sub>2</sub> film (21 nm TiO<sub>2</sub> particle) (X4,000) and (b) under large magnification (X40,000).

#### 4.1-2 Pore Morphology of TiO<sub>2</sub> Film

The pore characteristics (the pore size, pore size distribution, porosity and surface area) of TiO<sub>2</sub> film were measured by N<sub>2</sub> adsorption-desorption system (BET method) [98-100]. The adsorption-desorption standard isotherms for different porous types are shown in Figs. 4-3(a)-(f). These include (a) micro-porous sample, (b) non-porous sample, (c) macro-porous sample, (d) meso-porous sample, (e) micro-porous or meso-porous sample, and (f) sample with pores more than one type.

Micro-porous pore means that the pore size is smaller than 2 nm. Meso-porous pore means that the pore size is larger than 2 nm but smaller than 50 nm. Macro-porous pore means that the pore size is larger than 50 nm. [107] In general, one can determine the porous type of the sample by comparing the N<sub>2</sub> adsorption-desorption isotherm with the standard isotherms. However, the N<sub>2</sub> adsorption-desorption isotherms of our TiO<sub>2</sub> samples shown in Figs. 4-4(a) and (b) are different from the standard isotherms. The N<sub>2</sub> adsorption-desorption isotherms of TiO<sub>2</sub> films in this study appear to be a combination of Type 3 and Type 4 of the standard isotherms. This implies that the TiO<sub>2</sub> samples possess a bimodal distribution of meso- and macro-porous structures.

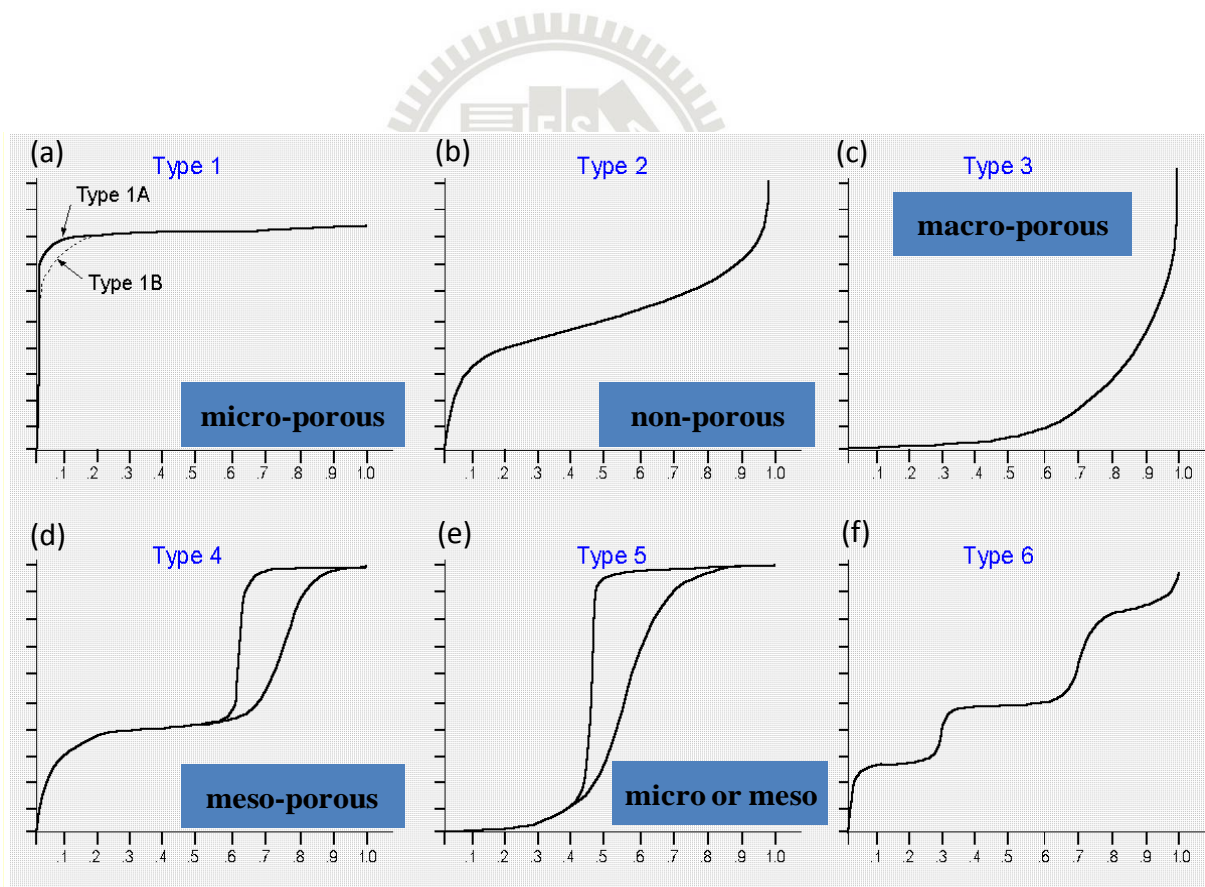


Fig. 4-3 N<sub>2</sub> adsorption-desorption standard isotherms for (a) micro-porous sample, (b) non-porous sample, (c) macro-porous sample, (d) meso-porous sample, (e) micro-porous or meso-porous sample and (f) sample with pores more than one type. [109]

The pore size distribution can be calculated by fitting the isotherm, for example, Fig. 4-4(a) using non local density functional theory (NLDFT) [100]. A bimodal pore size distribution is obtained and shown in Fig. 4-5 for the TiO<sub>2</sub> film prepared by paste using 15% PEG (MW = 35k) loading and H<sub>2</sub>O solvent. There exist two clear pore size distributions, namely 3~6 nm and 25~35 nm. It is also found that the N<sub>2</sub> adsorption-desorption isotherms for either butanol or water solvent show almost the same form. This indicates there is no difference in their macro-pore feature or distribution. This leads us to postulate that the extremely large pores originate from the voids and gaps between the TiO<sub>2</sub> film scraps in BET measurement.

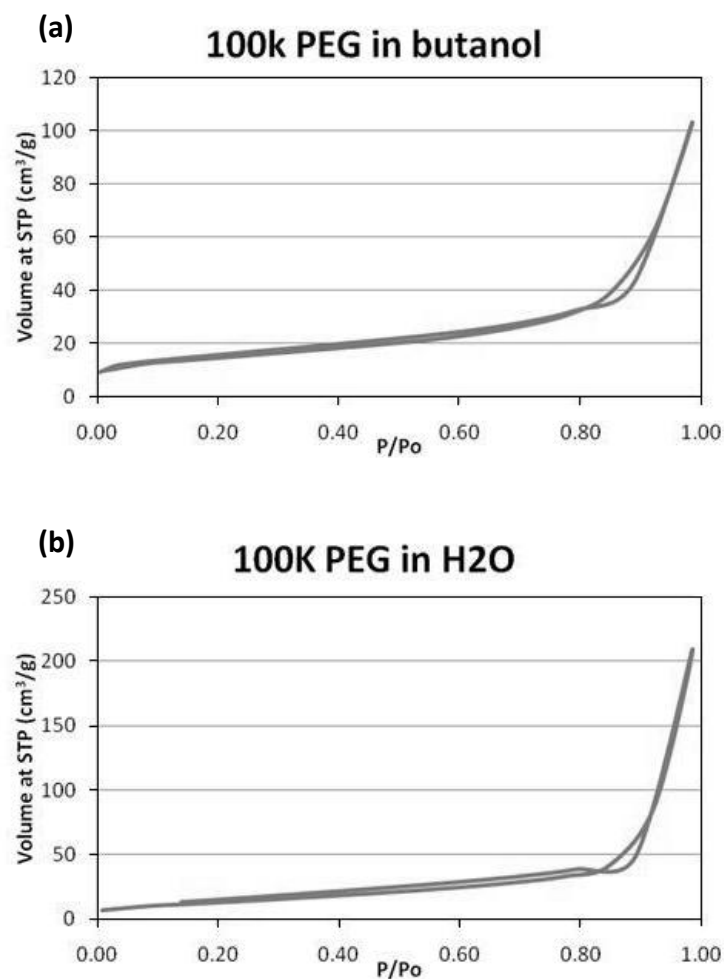


Fig. 4-4 The N<sub>2</sub> adsorption-desorption isotherms of the TiO<sub>2</sub> films prepared by TiO<sub>2</sub> paste in (a) butanol solution and (b) water solution.

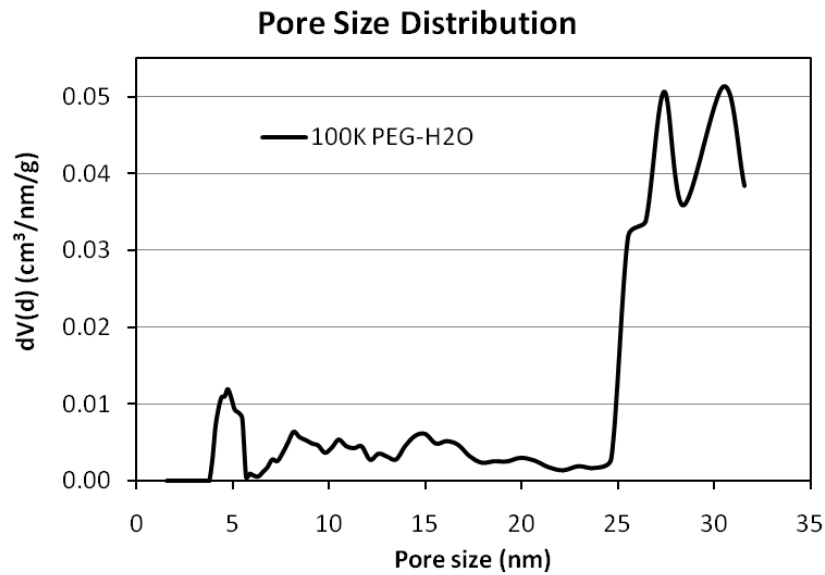


Fig. 4-5 A bimodal pore size distribution of the TiO<sub>2</sub> film prepared by paste using 15% PEG (MW = 100k) loading and H<sub>2</sub>O solvent

#### 4.1-2.1 Effects of PEG Molecular Weight and Loading on Pore Morphology of TiO<sub>2</sub> Films

##### (a) PEG loading

In order to understand the effects of molecular weight and loading of PEG in butanol solvent on the TiO<sub>2</sub> film morphology, the specific surface area, porosity, and average pore size are calculated from BET measurement and summarized in Table 4-1. After adding 5% PEG (MW=35k) in the TiO<sub>2</sub> paste, the porosity, surface area, and average pore size of TiO<sub>2</sub> films were increased from 31.05%, 52.72 m<sup>2</sup>/g, and 8.07 nm to 38.32%, 53.15 m<sup>2</sup>/g, and 10.91 nm, respectively. The porosity increased from 31.05% to 40.64% when PEG loading was increased to 15%, while the average pore size increased from 8.07 nm to 11.75 nm when PEG loading was increased from 5% to 15%. The increased porosity arises from the volume addition of PEG volume in TiO<sub>2</sub> paste through the formation of pores after burn-out of PEG porogen (pore generator). The configuration of PEG in the TiO<sub>2</sub> particles matrix will dictate the final

pore size after the removal of PEG at high temperature. The PEG in TiO<sub>2</sub> paste also acted as a surfactant, which could reduce the aggregation of TiO<sub>2</sub> nanoparticles, leading to a minor increase in surface area. It was found that the surface area and porosity of TiO<sub>2</sub> film only increased slightly after PEG addition. The TiO<sub>2</sub> film had the largest surface area when 10% PEG was added. It is believed that PEG addition could separate the TiO<sub>2</sub> particles, leading to increased surface area. However, the average pore size (10.9-11.8 nm) did not change much for various loadings of PEG/butanol in the TiO<sub>2</sub> paste.

#### **(b) Effect of molecular weight**

From Table 4-1, the average pore sizes of TiO<sub>2</sub> films were similar when PEG with different molecular weights (35k vs. 100k) were added in the TiO<sub>2</sub> paste. This is different from the study by Lee *et al.* [89]. In their study, the pore size increased with increasing molecular weight. Our difference is in the solvent system. Butanol in this study is a poor solvent for PEG. PEG molecules tend to curl in a poor solvent such that almost no difference of molecule sizes between 35k PEG and 100k PEG in the TiO<sub>2</sub> paste.

We changed the solvent system to water-based solvent, which is a good solvent for PEG molecules. The pore size distributions of TiO<sub>2</sub> films prepared by PEG with different molecular weights are shown in Fig. 4-6. The distribution for small pores shifted from 3~5 nm to 4~6 nm after replacing the paste solvent from butanol to water. For butanol system, PEG curled to a small coil size due to its poor solubility in butanol. And the pores became much larger in the TiO<sub>2</sub> film prepared by TiO<sub>2</sub> paste with 100k PEG addition in water solution because the PEG in water base paste could totally expand and take up larger in the TiO<sub>2</sub> matrix film after coating. The space taken up by PEG chains would turn into larger pores after burn-out.

Table 4-1 Pore morphology of TiO<sub>2</sub> film prepared by PEG with various molecular weights and loadings in butanol system paste.

	Surface Area (m <sup>2</sup> /g)	Average Pore Size (nm)	Pore Volume (cm <sup>3</sup> /g)	Porosity <sup>a</sup> (%)
0%PEG	52.72	8.07	0.1063	31.05
5% 35k PEG	53.15	10.91	0.1466	38.32
10% 35k PEG	57.18	11.89	0.1680	41.58
15% 35k PEG	54.47	11.75	0.1616	40.64
5% 100k PEG	53.03	11.57	0.1566	39.89
10% 100k PEG	57.51	11.74	0.1490	38.70
15% 100k PEG	54.90	11.69	0.1589	40.24

<sup>a</sup> Based on pore volume and 3.9 g/cm<sup>3</sup> of anatase TiO<sub>2</sub> density. Porosity (%) = pore volume (cm<sup>3</sup>/g) / (pore volume (cm<sup>3</sup>/g) + solid catalyst volume without pore (cm<sup>3</sup>/g)) × 100%. Solid catalyst volume without pore (cm<sup>3</sup>/g) = 1/ density of the solid catalyst without pore. [95]

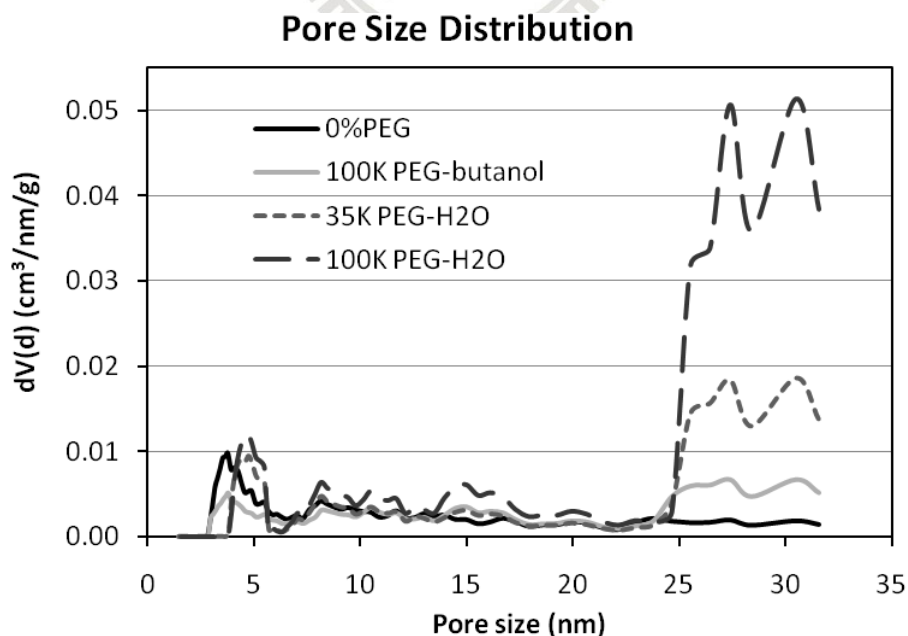


Fig. 4-6 The pore size distributions of the TiO<sub>2</sub> film produced by TiO<sub>2</sub> paste with 35k and 100k PEG addition and in different solvent system.

#### 4.1-2.2 Effect of solvents on Pore Morphology of TiO<sub>2</sub> Films

To further explore how to control the pore size of TiO<sub>2</sub> film, the effect of solvent on the pore morphology of TiO<sub>2</sub> films was investigated. Thus, a water-based solvent is chosen as a good solvent, while butanol-based solvent is selected as poor solvent for PEG in our comparative study. And 15% PEG loading was chosen because TiO<sub>2</sub> film would collapse if PEG loading is  $\geq 20\%$ .

#### Pore size distributions by BET measurement

The pore size distribution of TiO<sub>2</sub> films prepared by different solvent systems are shown in Fig. 4-7. From these distributions, it was found that the TiO<sub>2</sub> films were bimodal porous structures after PEG addition. The small pores had the distribution around 3~5 nm and large pores had the distribution around 25~35 nm. The small pores between TiO<sub>2</sub> particles were not affected by the addition PEG addition, while the large pores were enlarged by the addition of PEG. The PEG molecules in TiO<sub>2</sub> paste could enlarge the pores between TiO<sub>2</sub> particles, resulting in larger pores in TiO<sub>2</sub> films. When the solvent was changed from butanol to water, the small size pores shifted up slightly to 4~6 nm and the amount of large size pores increased significantly. The average pore size was increased from 11.8 nm (butanol, PEG 35k) to 22 nm (water, PEG 35k). The PEG expanded readily in the water-based TiO<sub>2</sub> paste and could produce larger pore between TiO<sub>2</sub> particles easily.

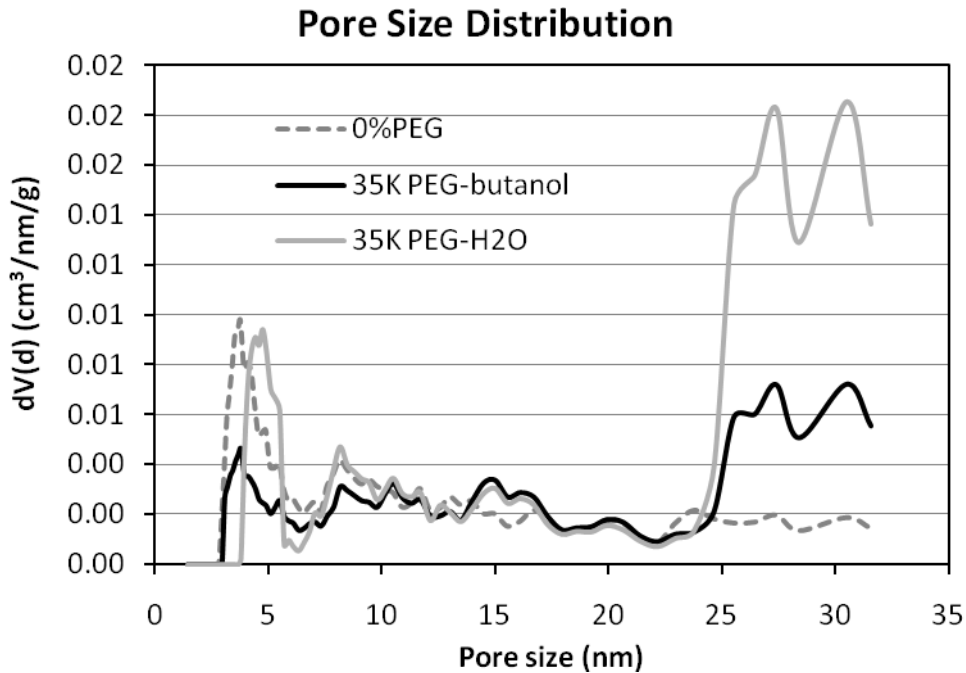


Fig. 4-7 The pore size distributions of the TiO<sub>2</sub> film produced by TiO<sub>2</sub> paste with 35k PEG in different solvent system.

The specific surface area, porosity, and average pore size of TiO<sub>2</sub> films using butanol and water solvents are calculated from BET measurement results and summarized in Table 4-2. There is substantial difference in the pore size and porosity of TiO<sub>2</sub> films between butanol and H<sub>2</sub>O solvents. TiO<sub>2</sub> films prepared by water-based TiO<sub>2</sub> paste possessed larger pore size and porosity as shown in Fig. 4-8. For 35k PEG case, the pore size increased from 11.75 nm in butanol system to 22.07 nm in water system, whose enlargement is 88%. Because of the ether groups in PEG molecules, PEG prefers to dissolve in the polar solvent. Therefore, solvent with a high dipole moment and dielectric constant would be an excellent solvent for PEG. The dipole moment and the dielectric constant of water are 1.85D and 80.1 for water, and 1.63D and 17.8 for butanol. [110] Also, the formation of hydrogen bonds in the solution affects the solubility. Water molecules can form more and stronger hydrogen bonding than butanol molecules with PEG in the solution because water molecules have more



polarized hydrogen to form hydrogen bonds with PEG. [111] That is the reason for higher solubility of PEG in water than in butanol.

To sum up, the large pore size in water-based solvent system is due to the large solubility of PEG, leading to full PEG chain extension in the TiO<sub>2</sub> particle matrix. Comparing water system with butanol (a poor solvent for PEG) system, the PEG molecules in water-based TiO<sub>2</sub> paste could modulate the structure of TiO<sub>2</sub> films with larger pores readily. The surface area increased ~8% from 54.5 (butanol) to 58.5 m<sup>2</sup>/g (water) because PEG could expand and disperse well in water solution and separate TiO<sub>2</sub> nanoparticles as a surfactant.

Table 4-2 Pore morphology of TiO<sub>2</sub> films prepared by PEG (15% loading; MW=35k or 100k) in different solvents

	Surface Area (m <sup>2</sup> /g)	Average Pore Size (nm)	Pore Volume (cm <sup>3</sup> /g)	Porosity (%)
0%PEG	52.72	8.07	0.1063	31.05
15% 35k PEG-butanol	54.47	11.75	0.1616	40.64
15% 100k PEG-butanol	54.90	11.69	0.1589	40.24
15% 35k PEG-H <sub>2</sub> O	58.54	22.07	0.2444	50.87
15% 100k PEG-H <sub>2</sub> O	57.51	30.50	0.5456	69.81

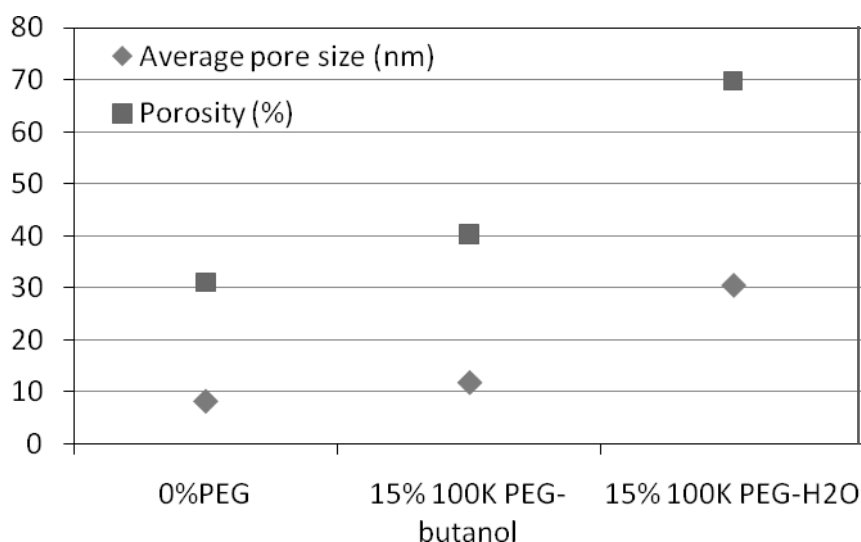


Fig. 4-8 Average pore size and porosity of TiO<sub>2</sub> films using different solvent systems

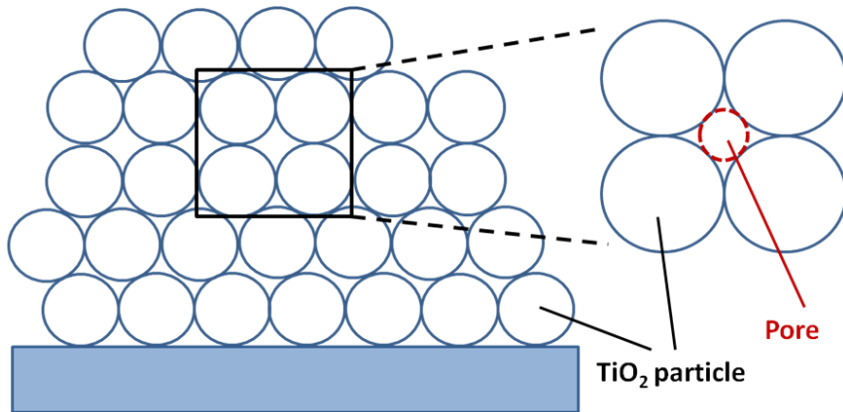
The PEG addition increased the porosity of TiO<sub>2</sub> films. PEG took up space in the TiO<sub>2</sub> particle matrix and contributed to the porosity after being burned out. Without solvents, PEG molecules would curl with itself and others closely. When PEG dissolved in butanol, a poor solvent for PEG, PEG curled chain would only expand slightly and the molecule volume would increase in TiO<sub>2</sub> particle matrix. This accounts for the little increase of TiO<sub>2</sub> film porosity with PEG addition. In water, which is a good solvent of PEG, the curled PEG chains would expand easily and take up more volume in TiO<sub>2</sub> particle matrix. Thus, the TiO<sub>2</sub> films prepared by water-based TiO<sub>2</sub> paste would have larger porosity.

The role of PEG as porogen (pore generator) in good (water) and poor (butanol) solvent and its mechanism controlling the porogen size (*i.e.* pore size after PEG burn-out) in the TiO<sub>2</sub> films are schematically illustrated in Fig. 4-9. The pore size is 8.1 nm when no PEG is added in the TiO<sub>2</sub> paste. The pores (~8 nm) are originated from the voids among the TiO<sub>2</sub> particles as shown in Fig. 4-9(a). When a poor solvent such as butanol is used, the average pore size is increased from 8.1 nm to ~11.8 nm when PEG with 35k or 100k MW is added into the TiO<sub>2</sub> paste. The molecular weight

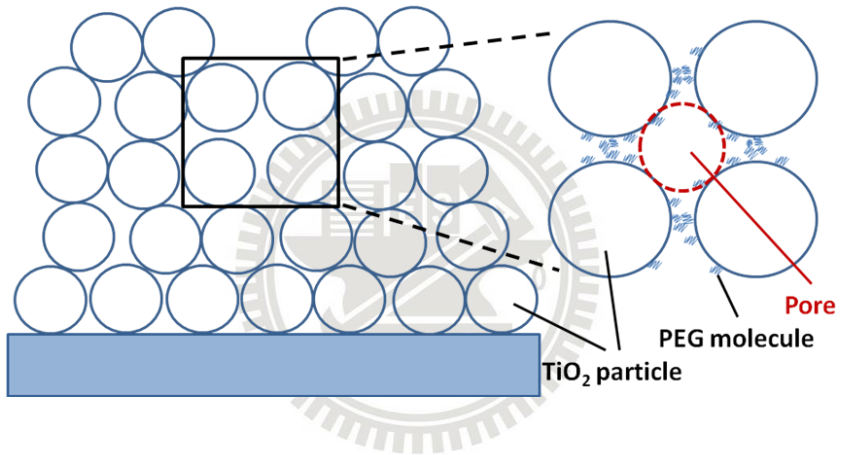
of PEG shows no impact on the pore size in  $\text{TiO}_2$  films because PEG chains tend to curl in butanol, a poor solvent and attach onto  $\text{TiO}_2$  nanoparticles. After burning out of PEG, the pore between particles is enlarged as illustrated in Fig. 4-9 (b). This is the reason for the same pore size in  $\text{TiO}_2$  films prepared by  $\text{TiO}_2$  paste with different molecular weight PEG in butanol. And in water solution as illustrated in Fig.4-9(c), the polymer chains of PEG tend to extend well and attach onto  $\text{TiO}_2$  particles. After PEG is burned out, the pore between particles would be further enlarged. When the PEG polymer chains are fully extended in water-based  $\text{TiO}_2$  paste, higher molecular weight shall lead to larger polymer coil size. Thus, the pore size is first increased to 22 nm for 35k PEG, then to 30.5 nm for 100k PEG as shown in Fig. 4-10.



**(a) TiO<sub>2</sub> film Without PEG**



**(b) TiO<sub>2</sub> film with PEG in poor solvent – PEG curl**



**(c) TiO<sub>2</sub> film with PEG in good solvent – PEG expand**

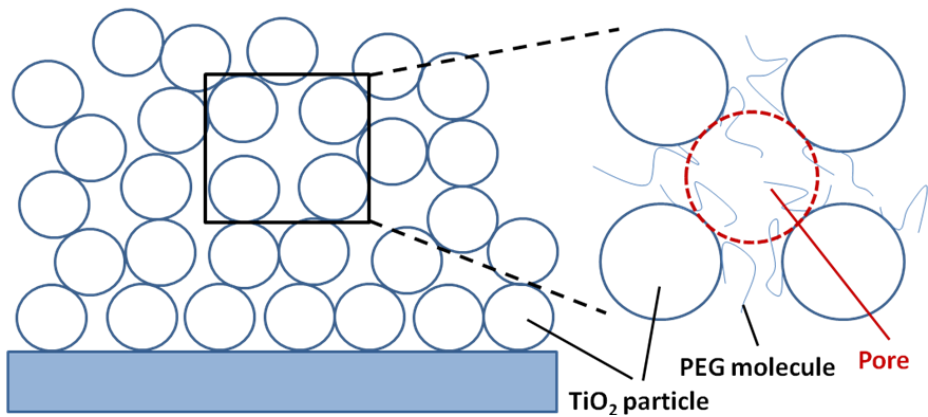


Fig. 4-9 Schematic diagram of PEG working mechanism in TiO<sub>2</sub> paste with different solvent systems. (a) TiO<sub>2</sub> film without PEG loading, (b) TiO<sub>2</sub> film with PEG loading in butanol solution, and (c) TiO<sub>2</sub> film with PEG loading in water solution.

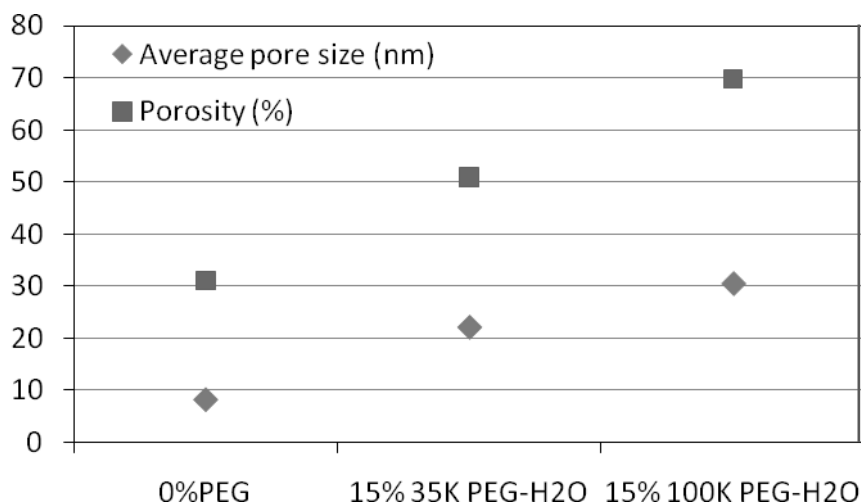


Fig. 4-10 Average pore size and porosity of TiO<sub>2</sub> films with different PEG molecular weight

#### 4.1-2.3 Effect of PEG Burn-out Rate on the Pore Morphology of TiO<sub>2</sub> Films

In addition to the use of PEG with different molecular weights as the porogen and surfactant to enhance surface area and pore size, we have shown that good solvent is effective to enlarge the pore size and surface area as discussed in previous sections. The other approach for controlling the pore size in TiO<sub>2</sub> films in this thesis is to change the PEG burn-out rate. So far, all porous TiO<sub>2</sub> films have been prepared by burning out PEG at 400 °C isothermally for 40 mins, which can be categorized as fast burn-out rate. For comparison, a slow PEG burn-out rate is carried out by baking the sample at 100°C for 30 minutes, then 400°C for 40mins.

The pore size distributions of the TiO<sub>2</sub> films prepared by different PEG burn-out processes are shown in Fig.4-11. The amount of small pore decreases, while the amount of large pores increases when a slow PEG burn-out rate is used. The same trend is observed for the average pore size. The enlarged pore size in slow burn-out rate case can be attributed to the chain expansion at additional isothermal step, 100°C

and possibly PEG aggregation.

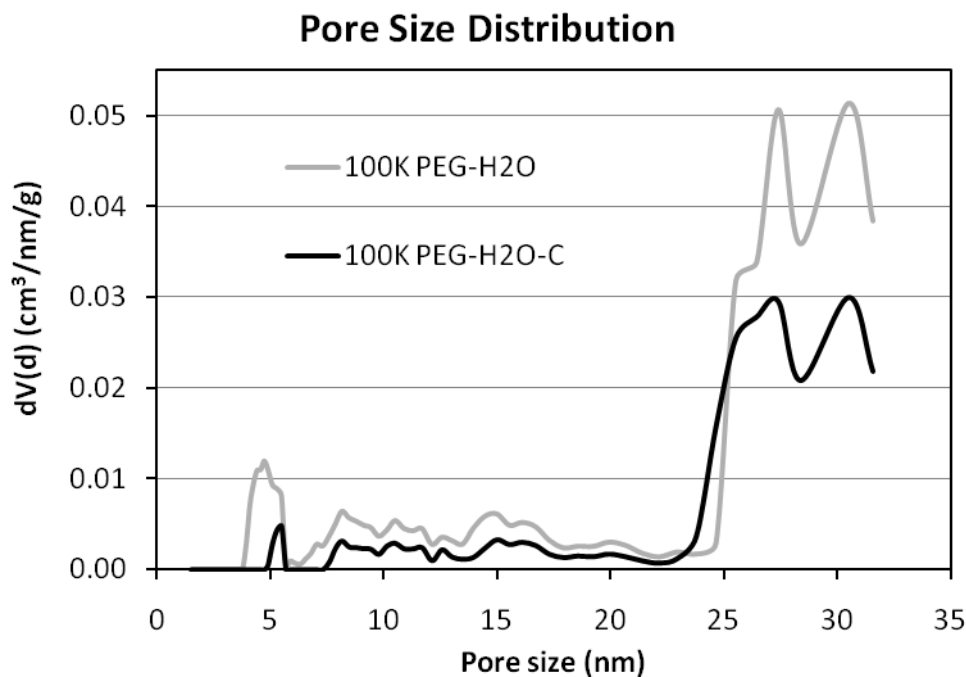


Fig. 4-11 The pore size distributions of the TiO<sub>2</sub> film prepared by different PEG burn-out rates using water-based pastes.

The increase of average pore size from 11 nm to 16 nm (an increase of 40%) in butanol system as shown in Fig. 4-12(a) was more than those in water system, from 22 nm to 24 nm (~9% increase) for 35k PEG and from 30 nm to 35 nm (~16% increase) for 100k PEG as shown in Fig.4-12(b) However, the porosity and surface decreased for 100k PEG as compared to 35k PEG as shows in Table 4-3. The reduction in porosity and surface area can be attributed to the TiO<sub>2</sub> film collapse caused by very large pores, which weakens the TiO<sub>2</sub> structure.

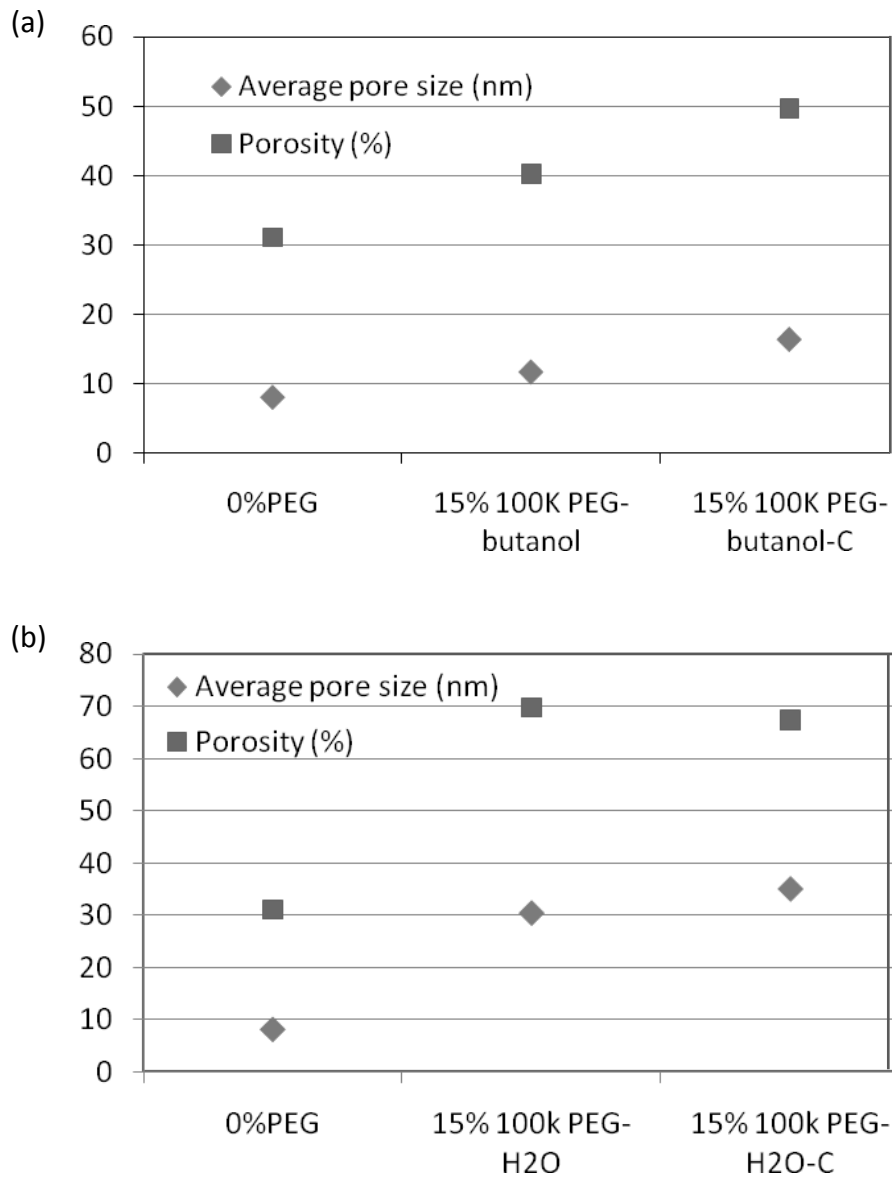


Fig. 4-12 (a) Average pore size and porosity of TiO<sub>2</sub> films with different PEG burn-out rates in butanol system (b) in water system

The specific surface area, porosity, and average pore size of TiO<sub>2</sub> films calculated from BET measurement are summarized in Table 4-3. The surface area, porosity, and average pore size increased when an additional isothermal bake at 100°C was implemented presumably due to the expansion of PEG polymer chains and possibly some degree of PEG chain aggregation. In contrast, PEG chains were decomposed readily without enough time for chain extension. This yielded smaller

pore size (11.8 nm for 35K PEG in butanol system, or 22.0 nm for 35k PEG in water system) under a fast burn-out rate at 400°C. The increase of average pore size from 11 nm to 16 nm (an increase of 40%) in butanol system was more than those in water system, from 22 nm to 24 nm (~9% increase) for 35k PEG and from 30 nm to 35 nm (~16% increase) for 100k PEG. It is believed that isothermal curing at 100°C provide energy for the curled PEG chains to expand readily, but only limited extension for PEG chains which are already in the extended mode. However, the porosity and surface decreased for 100k PEG as compared to 35k PEG. The reduction in porosity and surface area can be attributed to the TiO<sub>2</sub> film collapse caused by very large pores (> 30 nm), which weakens the TiO<sub>2</sub> structure. Overall, by combining water as solvent and slow burn-out rate for 35k PEG, the TiO<sub>2</sub> film with pore size 24.0 nm and porosity 60.07% possessed the largest surface area 59.12 m<sup>2</sup>/g in this study.

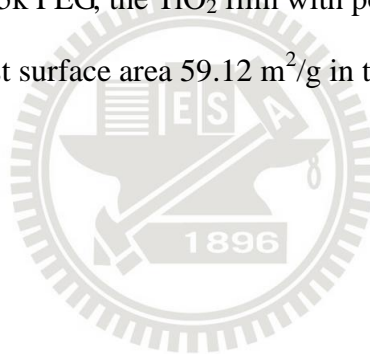




Table 4-3 Pore morphology of TiO<sub>2</sub> film prepared by PEG with various molecular weights and loading in butanol and water solvent systems and different PEG burn-out rates

	Surface Area (m <sup>2</sup> /g)	Average Pore Size (nm)	Pore Volume (cm <sup>3</sup> /g)	Porosity (%)
0%PEG	52.72	8.07	0.1063	31.05
15% 35k PEG-butanol	54.47	11.75	0.1616	40.64
15% 100k PEG-butanol	54.90	11.69	0.1589	40.24
15% 100k PEG-butanol-C <sup>a</sup>	56.87	16.36	0.2325	49.63
15% 35k PEG-H <sub>2</sub> O	58.54	22.07	0.2444	50.87
15% 35k PEG-H <sub>2</sub> O-C <sup>a</sup>	59.12	24.02	0.3550	60.07
15% 100k PEG-H <sub>2</sub> O	57.51	30.50	0.5456	69.81
15% 100k PEG-H <sub>2</sub> O-C <sup>a</sup>	55.46	35.13	0.4870	67.36

<sup>a</sup>The “-C” represent the TiO<sub>2</sub> film was prepared by a slow PEG burn-out process, which was baked at 100°C for 30 minutes, then at 400°C for 40 minutes to sinter TiO<sub>2</sub> and burn out PEG

### 4.1-3 Dye Adsorption Analysis

In order to determine the dye loadings in various TiO<sub>2</sub> films prepared by various PEG loadings, solvents, and burn-out rate, dye molecules were stripping off from the nominal TiO<sub>2</sub> electrodes using NaOH-water solution. The dye desorption amount was measured by UV-visible spectrum. From the spectra data, the dye adsorption of a TiO<sub>2</sub> film could be calculated by comparing the light absorption intensity of dye-desorbed NaOH solution and a reference NaOH solution. Here, Beer-Lambert law ((4-1) and (4-2)) is applied to calculate the dye adsorption within TiO<sub>2</sub> film.

$$T = \frac{I}{I_0} = 10^{-\alpha l} = 10^{-\epsilon c l} \quad (4-1)$$

$$A = -\log\left(\frac{I}{I_0}\right) = \epsilon c l \quad (4-2)$$

where T is light transmittance, I is the absorption intensity,  $\alpha$  is absorption coefficient, l is sample thickness, c is concentration,  $\epsilon$  is extinction coefficient, and A is light absorption.

As illustrated in Fig. 4-13, the absorbance intensity of reference solution with dye concentration  $8 \times 10^{-5} \text{M}$  at 491 nm was 0.521, while the absorbance intensity of the dye desorbed from the TiO<sub>2</sub> electrode into 5mM NaOH solution at 491 nm was 0.133. Using equation (4-2), the concentration of the solution, i.e. the dye adsorption on TiO<sub>2</sub> film, can be calculated after taking into account of the film thickness (19  $\mu\text{m}$  from SEM result. For TiO<sub>2</sub> electrode prepared by TiO<sub>2</sub> paste with 35k PEG loading in butanol system, the dye adsorption is  $3.88 \times 10^{-8}$  molecules per square centimeter.

The average pore size, porosity, UV-visible absorption intensity, calculated dye adsorption, and specific surface area of various TiO<sub>2</sub> films are summarized in Table 4-4. From Fig 4-14, the dye adsorption of various TiO<sub>2</sub> electrodes shows the same trend with the surface area as a function of pore sizes. This means that the dye

adsorption of TiO<sub>2</sub> electrode is mainly affected by surface area. But, the surface area and dye adsorption decreased when the pore size was larger than 30 nm because large pore and high porous structure would sacrifice the surface area. If compared these results with BET analysis results, we can also find that the dye adsorption almost has no correlation with the pore size and porosity. Moreover, the variation in the dye adsorption is very small compared to other study. [87]

Overall, by combining water as solvent and slow burn-out rate for 35k PEG, the TiO<sub>2</sub> film with pore size 24.0 nm and porosity 60.07% had the largest surface area 59.12 m<sup>2</sup>/g and highest dye absorption ( $4.89 \times 10^{-8}$  mol/cm<sup>2</sup>) as listed in Table 4.4.



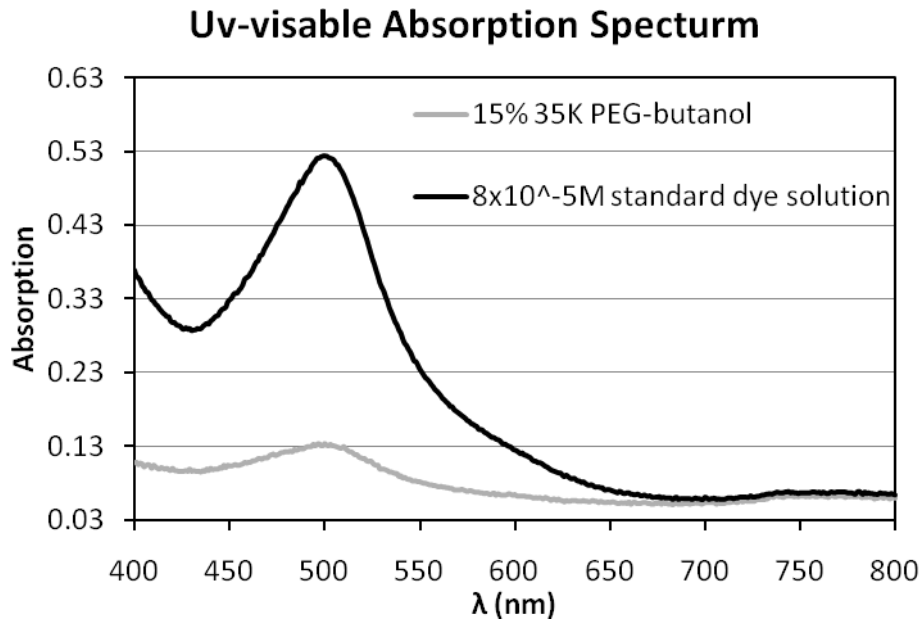


Fig. 4-13 UV-visible spectra of the reference dye solution and the dye desorption solution of TiO<sub>2</sub> film prepared by TiO<sub>2</sub> paste with 35k PEG loading in butanol system.

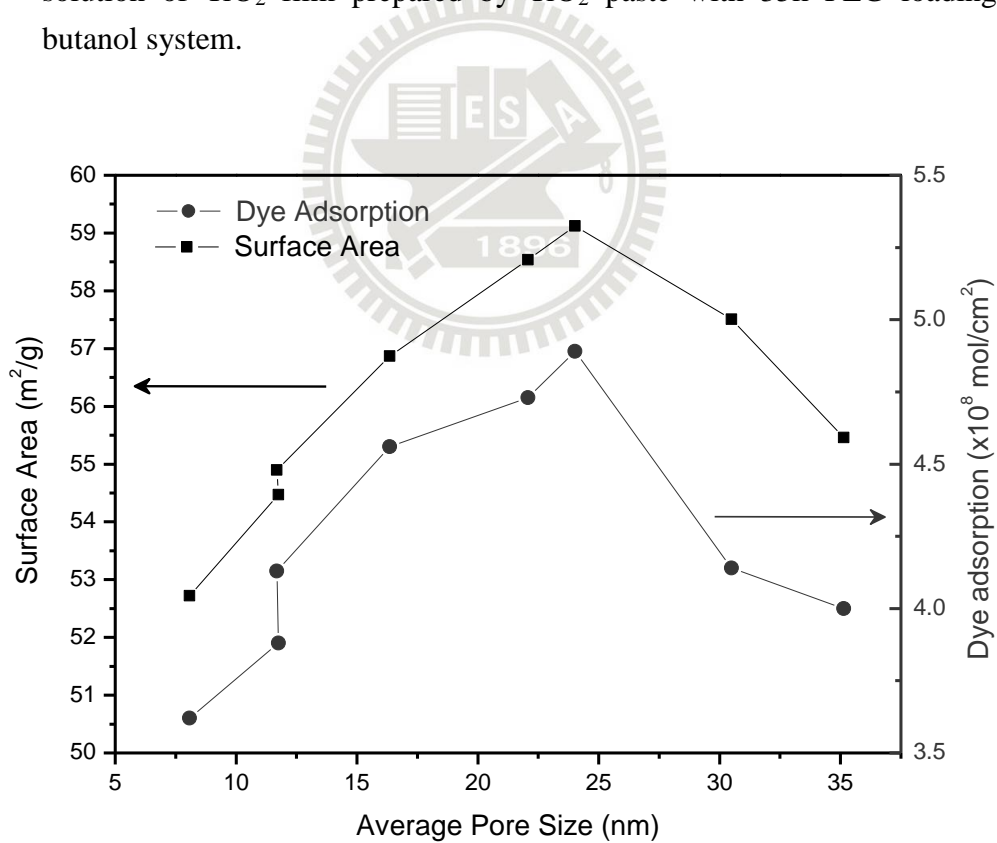


Fig. 4-14 Dye adsorption and surface area of TiO<sub>2</sub> films as a function of pore size

Table 4-4 Average pore size, UV-visible absorption intensity, dye adsorption, and specific surface area of various TiO<sub>2</sub> films.

	Average Pore Size (nm)	Absorption Intensity	Dye Adsorption ( $\times 10^{-8}$ mol/cm <sup>2</sup> )	Surface Area (m <sup>2</sup> /g)
0%PEG	8.07	0.124	3.62	52.72
15% 35k PEG-butanol	11.75	0.133	3.88	54.47
15% 100k PEG-butanol	11.69	0.142	4.13	54.90
15% 100k PEG-butanol-C	16.36	0.156	4.56	56.87
15% 35k PEG-H <sub>2</sub> O	22.07	0.162	4.73	58.54
15% 35k PEG-H <sub>2</sub> O-C	24.02	0.168	4.89	59.12
15% 100k PEG-H <sub>2</sub> O	30.50	0.142	4.14	57.51
15% 100k PEG-H <sub>2</sub> O-C	35.13	0.137	4.00	55.46



## 4.2 DSSC performance

### 4.2-1 Cell Efficiency

The TiO<sub>2</sub> electrodes with different pore morphologies were fabricated into DSSCs, whose active area was 0.28 cm<sup>2</sup>. The DSSC cell efficiency was characterized by scanning DSSC from -0.2V to 0.8V under AM1.5, 1 sun (100mW/cm<sup>2</sup>) solar simulator illumination, which is typically described as I-V curve. The fill factor (FF) and cell overall energy conversion efficiency ( $\eta$ ) were calculated from I-V curve by Eq.4-3 and Eq.4-4, which have been described in Chapter 2 in details.

$$FF = \frac{P_{MAX}}{V_{OC} \times I_{SC}} \quad (4-3)$$

$$\eta_{eff} = \frac{P_{MAX}}{P_{ill}} \times 100\% = \frac{V_{OC} \times I_{SC} \times FF}{P_{ill}} \times 100\% \quad (4-4)$$

Form this definition, we can see that the cell conversion efficiency affects by short circuit current density ( $J_{SC}$ ), open circuit voltage ( $V_{OC}$ ), and fill factor (FF). If discuss further, the short circuit current density usually affects by dye adsorption and light utilization. Open circuit voltage mainly affects by the TiO<sub>2</sub> row material property, such as energy band gap and crystalline phase. And fill factor is an efficiency factor, used for checking whether the  $P_{MAX}$  is ideally equal to  $V_{OC} \times I_{SC}$  or not. Thus, the fill factor would affect by many reasons such as how perfect the DSSC was sealed or how fast the reactions react in DSSCs.

For example, the I-V curve of DSSC with TiO<sub>2</sub> electrode prepared by PEG (15% loading, 35k) in butanol solvent is shown in Fig. 4-15. In addition, the schematic drawing for the efficiency calculation is illustrated. From I-V curve, the open circuit voltage ( $V_{OC}$ ) is 0.73V and the short circuit current density ( $J_{SC}$ ), 11.91 mA/cm<sup>2</sup>, which is obtained from the short circuit current ( $I_{SC}$ ), 3.34 mA dividing by the active area 0.28 cm<sup>2</sup>. And the maximum power ( $P_{MAX}$ ) is obtained from the maximum ( $I \times$

V) value, which is  $9.74 \times 0.48$  for the case shown in Fig.4-16. Applying the Eqs. (4-3) and (4-4), the fill factor (FF) and conversion efficiency ( $\eta$ ) of DSSC with  $\text{TiO}_2$  electrode prepared by 35k PEG at 15% loading  $\text{TiO}_2$  paste in butanol system are 0.54 and 4.97%, respectively.

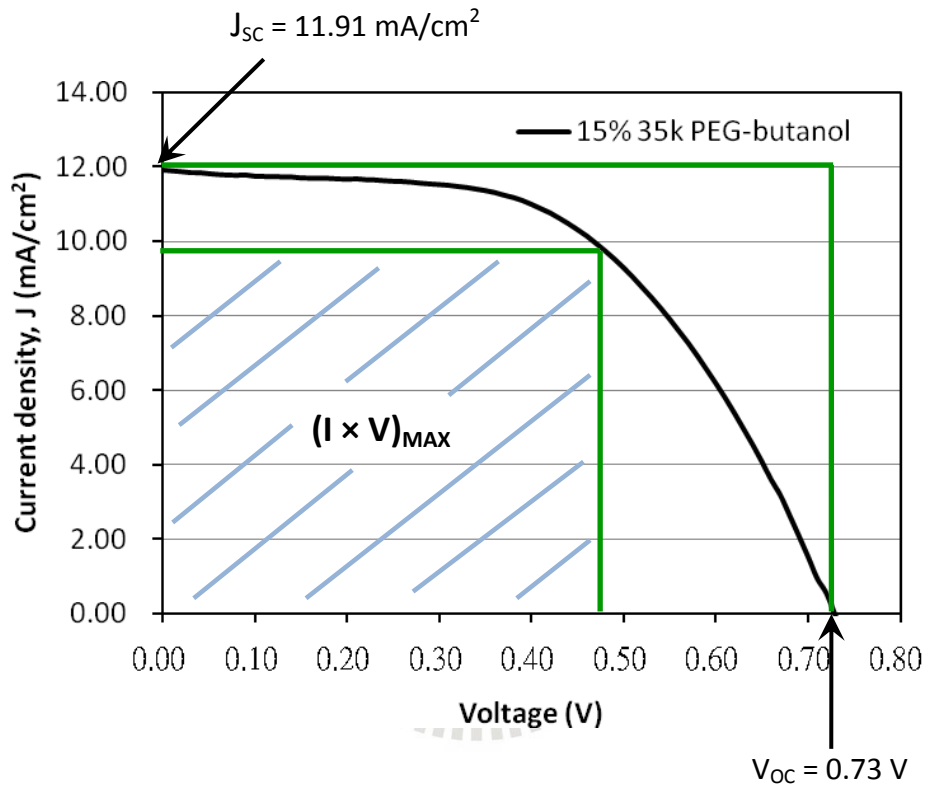


Fig. 4-15 I-V curve of DSSC with  $\text{TiO}_2$  electrode prepared by PEG (35k, 15% loading)  $\text{TiO}_2$  paste in butanol system.

The I-V curves of DSSCs with  $\text{TiO}_2$  electrode prepared by  $\text{TiO}_2$  paste with no PEG loading, 35k PEG 15% loading in water system, and 100k PEG 15% loading in water system combined with slow PEG burn-out process are shown in Fig.4-16. The latter two cases show the highest and lowest DSSC efficiency in this study, respectively. Therefore, they are highlighted for comparison and discussion relative to control DSSC without adding PEG.

The PEG adding into water system  $\text{TiO}_2$  paste increased the short circuit current

density ( $J_{sc}$ ), open circuit voltage ( $V_{oc}$ ), and fill factor (FF) because the surface area, pore size and porosity in  $TiO_2$  film increased. More surface area adsorbed more dye molecules and mainly increased the short circuit current density. [93, 108] With larger pore size and porosity in  $TiO_2$  films, electrolyte diffusion became easier, which improved the regeneration of dye and increase the fill factor. [14, 95, 97] Also, the large pore could act as light scattering center to increase light scattering inside the DSSC and improved the photon-electron conversion. [10, 96] For  $TiO_2$  electrode prepared by 15% 100k PEG loading in water system combined with a slow PEG burn-out rate, its short circuit current density ( $J_{sc}$ ) of DSSC was even smaller than that of a control DSSC without PEG addition. The low  $J_{sc}$  can be attributed to the film collapse due to the large and weaken pores and the reduced surface area of  $TiO_2$ . The damage of film caused difficult charge transfer in  $TiO_2$  film, which decreased the short circuit current density ( $J_{sc}$ ). [11]

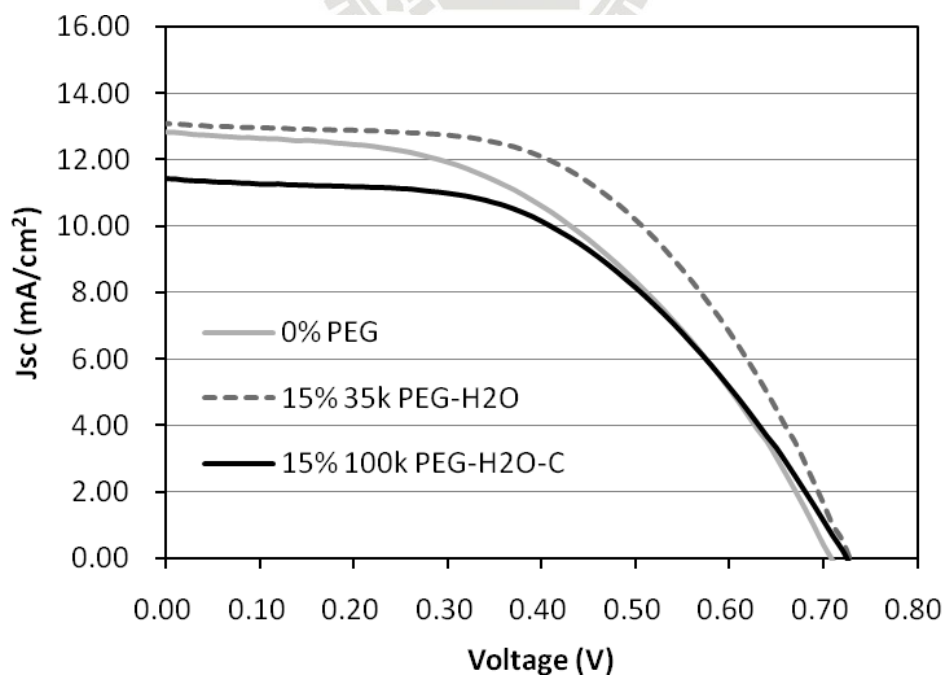


Fig. 4-16 I-V curves of DSSCs with  $TiO_2$  electrode prepared by  $TiO_2$  paste with no PEG loading, 35k PEG 15% loading in water system, and 100k PEG 15% loading in water system combined with slow PEG burn-out process.



The DSSC performances of other TiO<sub>2</sub> electrodes are summarized in Table 4-5. From the results, the short circuit current density and the fill factor were greatly affected by different TiO<sub>2</sub> morphology. Among various DSSCs, DSSC with TiO<sub>2</sub> electrode prepared by 15% 35k PEG loading paste in water system shows higher short current density and fill factor than all the others. The short circuit current density ( $J_{SC}$ ), the fill factor (FF), and the open circuit voltage ( $V_{OC}$ ) are 13.07 mA/cm<sup>2</sup>, 0.54, and 0.73V, respectively to yield the highest efficiency ( $\eta$ ), 5.13%. This TiO<sub>2</sub> electrode had surface area of 58.54 m<sup>2</sup>/g, pore size of 22.07 nm, and porosity of 50.87%.

For the all DSSCs in this study, the fill factor was increased from 0.47 to 0.54 after the addition of PEG into TiO<sub>2</sub> paste. The 15% increase of fill factor was the main improvement for DSSC conversion efficiency in our experiment. These TiO<sub>2</sub> electrodes with larger pore size and porosity could make electrolyte diffusion easier in the TiO<sub>2</sub> films. Better electrolyte diffusion led to faster dye regeneration and better efficiency in the photocurrent conversion, which increased not only the fill factor but also the DSSC cell performance. [11, 95, 96] The short circuit current density ( $J_{SC}$ ) was increased to 13.07 mA/cm<sup>2</sup> presumably due to more adsorbed dye molecules from higher surface area with the incorporation of pores. More dye molecules can generate more photocurrent and increase the DSSC conversion efficiency. [94]

However, in the case of the DSSC with larger pore size than 24 nm and porosity larger than 60%, the short circuit current density was reduced to 11.1-11.7 mA/cm<sup>2</sup>. The decrease in  $J_{SC}$  could be attributed to large numbers of oversized pores, which make the charge transfer in TiO<sub>2</sub> film difficult and enhance the electron/hole recombination reaction at electrolyte and FTO conducting electrode interface and TiO<sub>2</sub>/dye/electrolyte interface. Overall, the charge recombination and loss of photocurrent reduced the short circuit current density and cell conversion efficiency.

[76, 90, 96] Furthermore, in the case of DSSC with TiO<sub>2</sub> electrode prepared by 15% 100k PEG loading in water system combined with a slow PEG bun-out rate process, the fill factor dropped to 0.5 because the oversized pores caused film collapse and damaged the TiO<sub>2</sub> electrode. The damage in TiO<sub>2</sub> films weakened the connection of nanostructure and retarded the charge transfer in TiO<sub>2</sub> film. This made the cell conversion efficiency decrease to 4.17, which was even lower than that of control DSSC (without PEG addition).

Table 4-5 Photovoltaic characteristics of DSSCs made by different TiO<sub>2</sub> electrodes.

	V <sub>OC</sub> (V)	J <sub>SC</sub> (mA/cm <sup>2</sup> )	FF	η (%)
0%PEG	0.71	12.81	0.47	4.31
15% 35k PEG-butanol	0.73	11.91	0.54	4.67
15% 100k PEG-butanol	0.73	12.63	0.53	4.85
15% 100k PEG-butanol-C	0.74	12.81	0.54	5.09
15% 35k PEG-H <sub>2</sub> O	0.73	13.07	0.54	5.13
15% 35k PEG-H <sub>2</sub> O-C	0.74	11.67	0.52	4.46
15% 100k PEG-H <sub>2</sub> O	0.72	11.14	0.54	4.36
15% 100k PEG-H <sub>2</sub> O-C	0.73	11.41	0.50	4.17

#### 4.2-2 Impedance inside DSSCs

The impedances between various interfaces inside DSSC were measured by electrochemical impedance spectroscopy (EIS) and reported in the form of the Nyquist plots. There are four internal impedances in the DSSC, which have great effects on the electron transport in the DSSC. Fig. 4-17 shows an EIS spectrum (Nyquist diagram) of DSSC with  $\text{TiO}_2$  electrode prepared by PEG (35k, 15% loading-water paste under illumination. This Nyquist diagram shows three semicircles related to  $R_1$ ,  $R_2$ , and  $R_3$  of a typical DSSC. The resistance ( $R_1$ ) is related to the charge transfer at the platinum counter electrode. The resistance ( $R_2$ ) is related to the electron transport in the  $\text{TiO}_2$ /dye/electrolyte interface, while the resistance ( $R_3$ ) is related to Nernstian diffusion within the electrolyte in the low-frequency. [15, 19] The fourth internal impedance is represented as the resistance ( $R_s$ ), which is related to the sheet resistance of the FTO and electrolyte in the high frequency range. In order to obtain these resistances ( $R_1$  through  $R_4$ ), an equivalent circuit illustrated in Fig. 4-18 was used to simulate and fit the Nyquist diagram. [15]

The sheet resistance of the FTO and electrolyte in the high frequency range ( $R_s$ ) is usually related to the sealing process and external circuit. Moreover, the charge transfer resistance at the platinum counter electrode ( $R_1$ ) is related to the counter electrode material and electrolyte. Since these two resistances ( $R_s$  and  $R_1$ ) are not affected by the  $\text{TiO}_2$  electrode, they will not be examined further in this study.

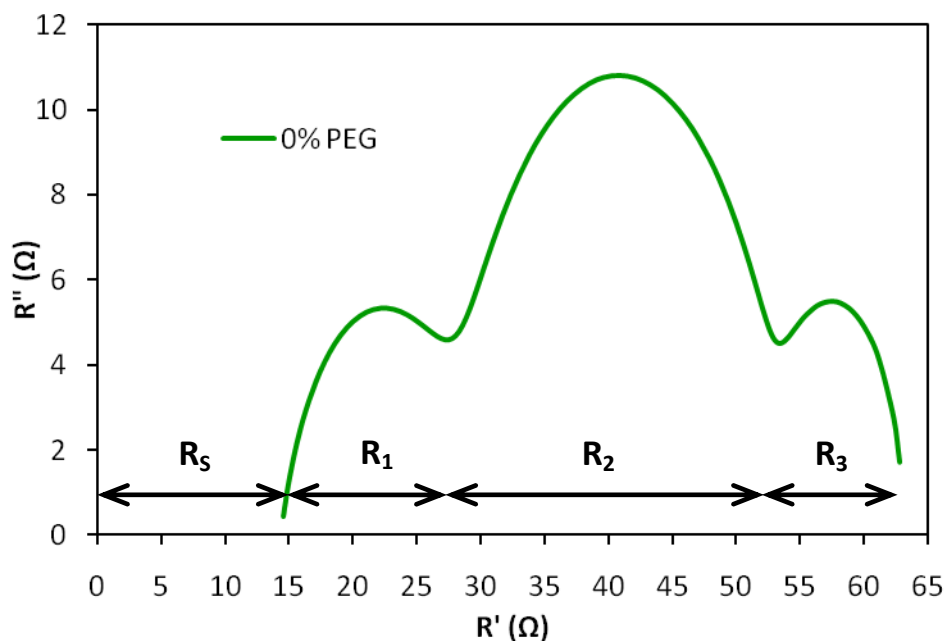


Fig. 4-17 An EIS spectrum (Nyquist diagram) of DSSC with  $\text{TiO}_2$  electrode prepared by PEG (35k, 15% loading)-water paste under illumination

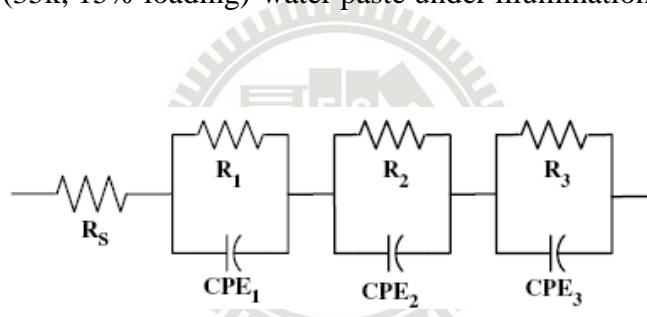


Fig. 4-18 The equivalent circuit for the DSSC

Fig. 4-19 shows the EIS spectra of DSSC with  $\text{TiO}_2$  electrode prepared by  $\text{TiO}_2$  paste with (1) no PEG loading, (2) PEG (35k, 15% loading) in water system, and (3) PEG (100k, 15% loading) in water system combined with a slow PEG burn-out process. The DSSC with  $\text{TiO}_2$  electrode prepared by 15% 35k PEG loading water system paste has smallest  $R_2$  and  $R_3$ , which means charge transfer at  $\text{TiO}_2/\text{dye}/\text{electrolyte}$  interface and redox couple diffusion in electrolyte were easiest. [95]  $R_2$  of DSSC with  $\text{TiO}_2$  electrode prepared by 15% 100k PEG loading in water system followed with the controlled the PEG burn out process became large again, and was even larger than DSSC with  $\text{TiO}_2$  electrode without PEG adding. That means

the charge transfer at  $\text{TiO}_2/\text{dye}/\text{electrode}$  interface become difficult which caused by weak linkage nanostructure of the  $\text{TiO}_2$  film with overlarge pores. [11, 96]

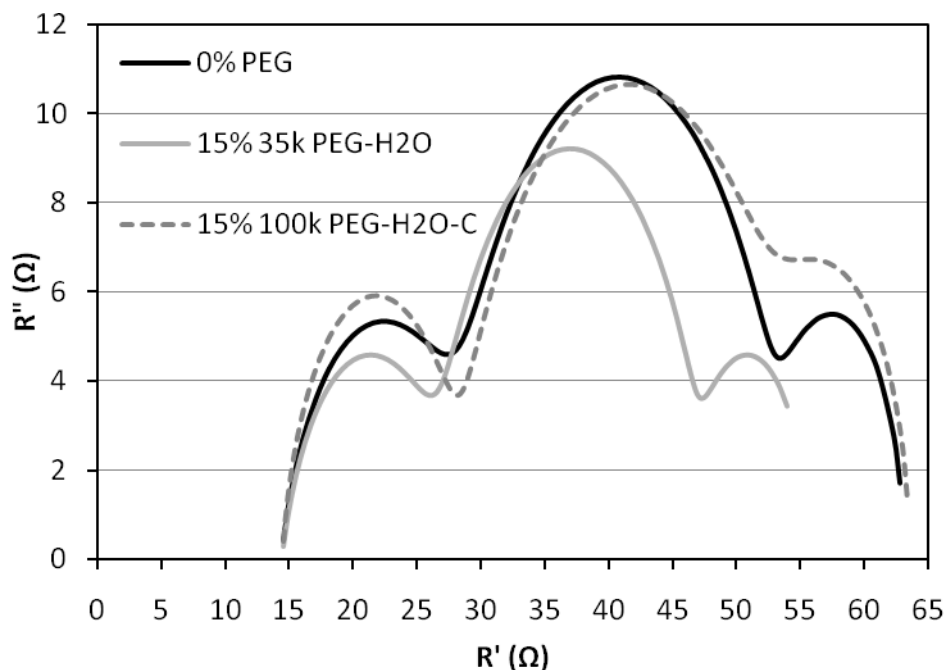


Fig. 4-19 EIS spectra of DSSC with  $\text{TiO}_2$  electrode prepared by  $\text{TiO}_2$  paste with (1) no PEG loading, (2) PEG (35k, 15% loading) in water system, and (3) PEG (100k, 15% loading) in water system combined with a slow PEG burn-out process.

The average pore size and porosity in  $\text{TiO}_2$  film, fitted impedance parameters and conversion efficiency of DSSCs with different  $\text{TiO}_2$  electrodes are summarized in Table 4-6, and drawn into figures for comparing. For butanol-based  $\text{TiO}_2$  pastes, both  $R_2$  and  $R_3$  resistances were slightly reduced upon the addition of PEG (35k/100k, 15% loading) because of a small increase of the average pore sizes from 8 nm to 11.7 nm. In contrast, for water-based  $\text{TiO}_2$  pastes, both  $R_2$  and  $R_3$  resistances were much reduced upon the addition of PEG (35k, 15% loading) whose pore size was 22.07 nm, as compared to control DSSC (0% PEG) with a pore size of 8 nm. But, both  $R_2$  and  $R_3$  resistances were increased again if the pore size became too large ( $\geq 24$  nm) when

higher MW and/or a slow PEG burn-out rate were used.

In specific, the DSSC with TiO<sub>2</sub> electrode prepared by PEG (35k, 15% loading)-water paste possessed the smallest R<sub>2</sub> and R<sub>3</sub>, 20.07Ω and 8.32Ω. The R<sub>2</sub> and R<sub>3</sub> decrease with pore size and porosity, if the pore size smaller than 24nm and porosity less than 60%. The smaller R<sub>2</sub> implies a better charge transfer at TiO<sub>2</sub>/dye/electrolyte interface because (1) the electrolyte can diffuse more easily in larger pores and more porous nanostructure can regenerate the dye faster, and (2) more adsorbed dyes on TiO<sub>2</sub> surface can generate more photoelectrons. Smaller R<sub>3</sub> means better redox couples diffusion in the electrolyte because larger pore can make electrolyte diffusion more easily. [95, 96] From figure 4-20, 4-21 and 4-22, we can find that R<sub>2</sub>, R<sub>3</sub> and cell efficiency mainly depended on pore size and porosity, and little depended on surface area. Thus, the decrease of R<sub>2</sub> was because larger pores and more porous nanostructure can let electrolyte diffuse more easily and regenerate the dye faster.

Table 4- 6 Average pore size and porosity in TiO<sub>2</sub> film, fitted impedance parameters and conversion efficiency of DSSCs with different TiO<sub>2</sub> electrodes.

	Average Pore Size (nm)	Porosity (%)	η (%)	R <sub>2</sub> (Ω)	R <sub>3</sub> (Ω)
0%PEG	8.07	31.05	4.31	24.92	10.21
15% 35k PEG-butanol	11.75	40.64	4.67	24.36	10.97
15% 100k PEG-butanol	11.69	40.24	4.85	22.06	9.52
15% 100k PEG-butanol-C	16.36	49.63	5.09	21.2	8.32
15% 35k PEG-H <sub>2</sub> O	22.07	50.87	5.13	20.07	8.32
15% 35k PEG-H <sub>2</sub> O-C	24.02	60.07	4.46	22.69	8.82
15% 100k PEG-H <sub>2</sub> O	30.50	69.81	4.36	24.39	9.15
15% 100k PEG-H <sub>2</sub> O-C	35.13	67.36	4.17	25.71	9.59

The resistances, especially  $R_2$  increased when the  $\text{TiO}_2$  pore size larger than 24 nm and porosity larger than 60%. This means the overlarge pore and porosity would make the charge transfer at the  $\text{TiO}_2/\text{dye}/\text{electrolyte}$  interface difficult. It is because oversized pores may enhance the electron/hole recombination reaction due to fast electrolyte diffusion and reduce charge transfer because of the reduced  $\text{TiO}_2$  connectivity. In the case of DSSC with  $\text{TiO}_2$  electrode prepared by PEG (100k, 15% loading) in water system combined with a slow PEG burn-out rate process, the total resistances are even larger than the control DSSC (0% PEG). The much higher resistance,  $R_2$  can be attributed to the over-sized pores (35 nm) and film collapse, which make the charge transfer difficult and enhance the electron/hole recombination reaction. [11, 96]

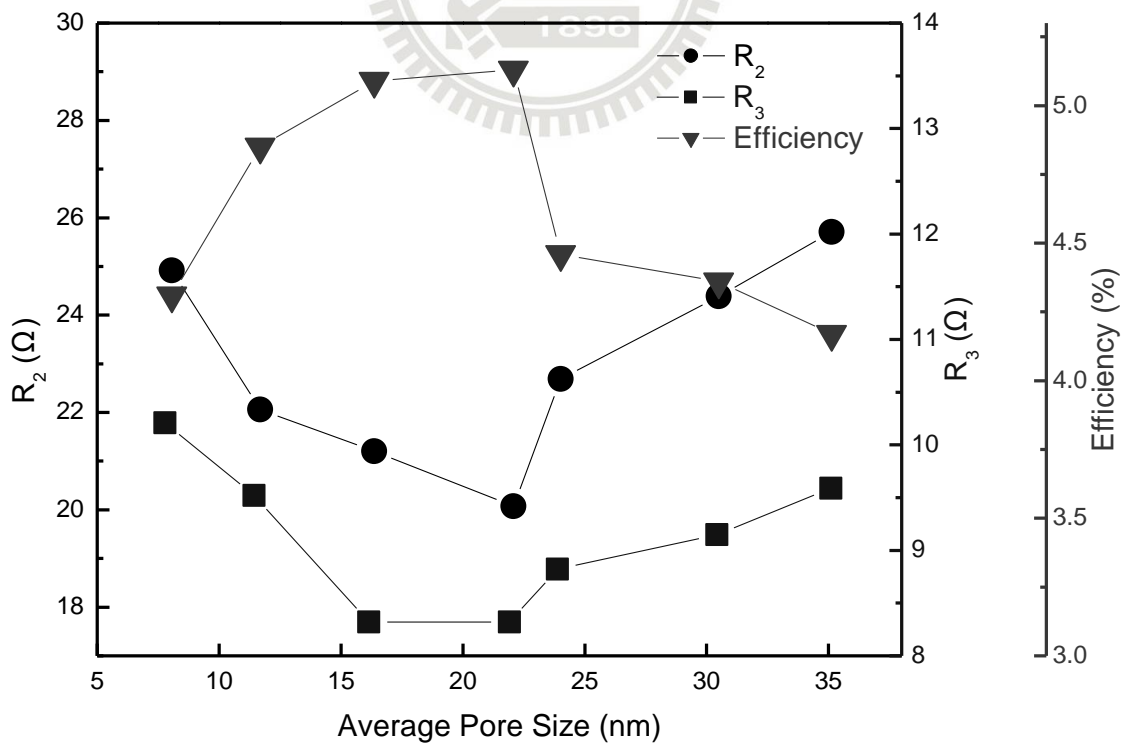


Fig. 4-20  $R_2$ ,  $R_3$  and efficiency of DSSCs with different pore size  $\text{TiO}_2$  films

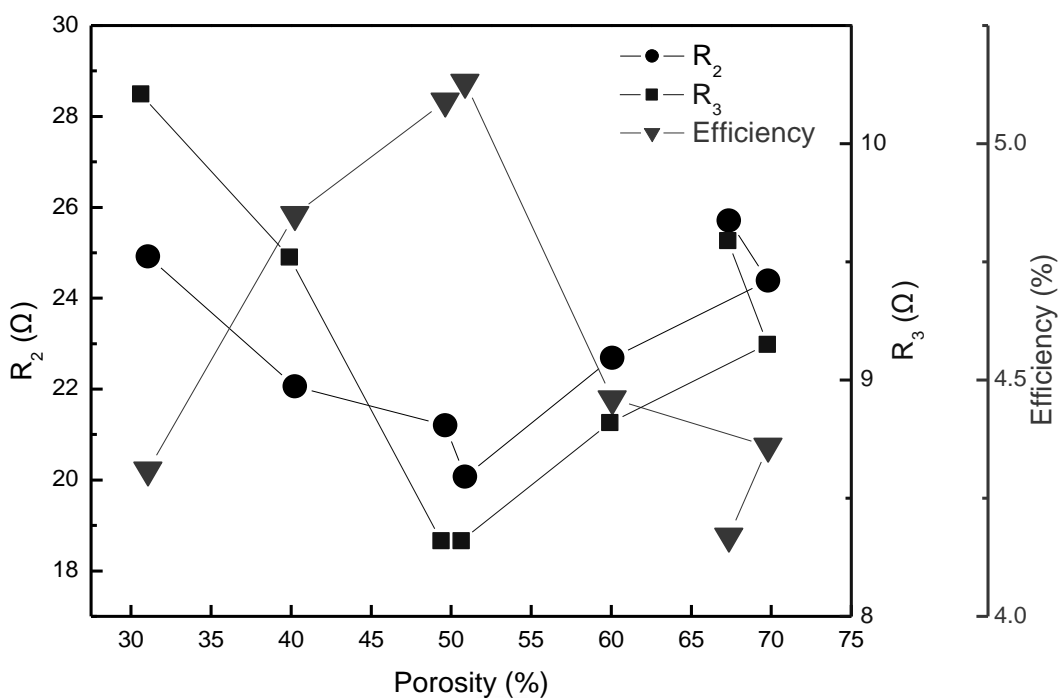


Fig. 4-21 R<sub>2</sub>, R<sub>3</sub> and efficiency of DSSCs with different porosity TiO<sub>2</sub> films

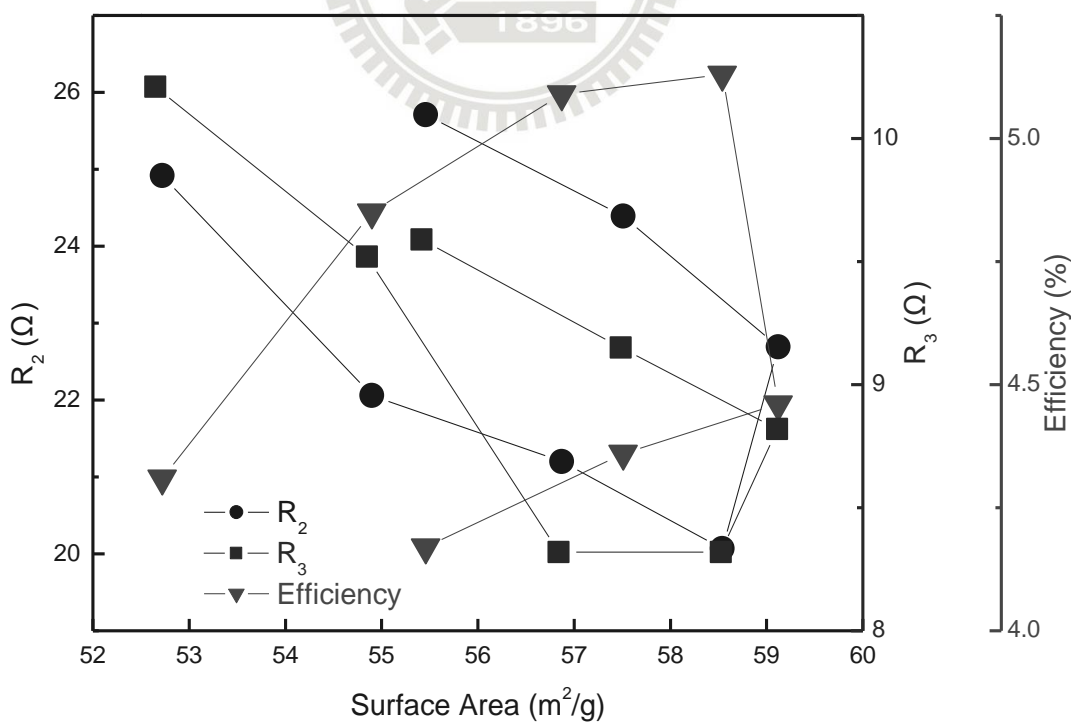


Fig. 4-22 R<sub>2</sub>, R<sub>3</sub> and efficiency of DSSCs with different surface area TiO<sub>2</sub> films



## Chapter 5 Conclusion

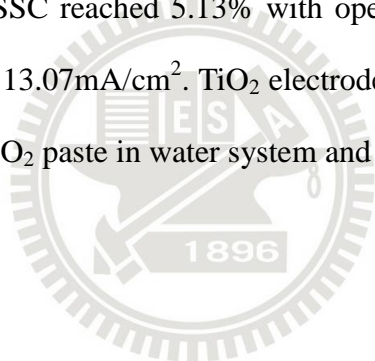
In order to modify the pore morphology of  $\text{TiO}_2$  (pore size, surface area, and porosity) to improve the DSSC performance, solvents and PEG in different molecular weights and loadings were added to  $\text{TiO}_2$  paste, in addition to using different PEG burn out rate after  $\text{TiO}_2$  films coating. In specific,  $\text{TiO}_2$  films with different pore morphology were prepared by coating commercial  $\text{TiO}_2$  nanoparticles (P25) and a scattering layer on FTO conducting glass using doctor-blade technique. The surface area, porosity, and pore size of  $\text{TiO}_2$  films and the photochemical characteristics of DSSCs with these  $\text{TiO}_2$  films have been examined by SEM, BET, and EIS analysis.

Results showed that PEG addition could separate the  $\text{TiO}_2$  particles leading to modify the pore morphology of  $\text{TiO}_2$ . In butanol based solvent, the surface area, pore size and porosity of  $\text{TiO}_2$  film only increased slightly because butanol is a poor solvent for PEG, and PEG molecules tend to curl in a poor solvent. Even changed the molecular weights, there was almost no difference of molecule sizes in the  $\text{TiO}_2$  paste. When the solvent was changed from butanol to water, the average pore size was increased from 11.8 nm to 22 nm due to the large solubility of PEG leading full PEG chain extension in the  $\text{TiO}_2$  particle matrix. And the molecular weights adjusting in water solution increased the pore size from 22 nm for 35k PEG to 30.5 nm for 100k PEG. Because the PEG porogen (pore generator) in good solvent (water) leading the polymer chains of PEG tend to extend well, as the PEG polymer chains are fully extended in water-based  $\text{TiO}_2$  paste, higher molecular weight shall lead to larger polymer coil size.

In addition to using different solvents and molecular weights of PEG, burn out rate is another issue to modify the pore morphology of  $\text{TiO}_2$ . When an additional

isothermal bake at 100°C the average pore size increased due to the expansion of PEG polymer chains and possibly some degree of PEG chain aggregation. In contrast, PEG chains were decomposed readily without enough time for chain extension. This yielded smaller pore size (11.8 nm for 35K PEG in butanol system, or 22.0 nm for 35k PEG in water system) under a fast burn-out rate at 400°C.

Applying these pore morphology modified TiO<sub>2</sub> films to DSSCs. By PEG addition, the conversion efficiency of DSSC increased with increasing pore size because electrolyte diffuse more easily in large pore size TiO<sub>2</sub> films led to faster dye regeneration, and the electron transport resistance in the TiO<sub>2</sub>/dye/electrolyte interface ( $R_2$ ) and the resistance ( $R_3$ ) of Nernstian diffusion decreased. In this study, the best conversion efficiency of DSSC reached 5.13% with open circuit voltage 0.73V and short circuit current density 13.07mA/cm<sup>2</sup>. TiO<sub>2</sub> electrode of this DSSC was prepared by 15% 35k PEG loading TiO<sub>2</sub> paste in water system and the average pore size was 22 nm.



## Reference

---

- [1] M. Grätzel, *Nature*, **414**, 338 (2001)
- [2] 李佳徽, “ Synthesis of Pt/Ni Bimetallic Nanoparticles and Its Application in Dye-Sensitized Solar Cells”, National Tsing Hua University, master thesis (2008)
- [3] Newport Corporation Website
- [4] B. O'Regan and M. Grätzel, *Nature*, **353**, 737 (1991)
- [5] M. Grätzel, *J. Photochem. Photobiol. A*, **164**, 3 (2004)
- [6] M. Grätzel, *Prog. Photovoltaics*, **14**, 429 (2006)
- [7] Q. Shen and T. Toyoda, *Thin Solid Films* **167** 438 (2003)
- [8] S. Ngamsinlapasathian, S. Sakulphaemaruehai, S. Pavasupree, A. Kitiyanan, T. Sreethawong, Y. Suzuki, and S. Yoshikawa, *J. Photochem. Photobiol. A***164**, 145 (2004)
- [9] G. K. Mor, O. K. Varghese, M. Paulose, K. Shankar, and C. A. Grimes, *Sol. Energy Mater. Sol. Cells* **90**, 2011 (2006)
- [10] S. Hore, P. Nitz, C. Vetter, C. Prah, M. Niggemann, and R. Kern, *Chem. Commun.*, **41**, 2011 (2005)
- [11] J. Li, L. Wang, X. Kong, B. Ma, Y. Shi, C. Zhan, and Y. Qiu, *Langmuir* **25**, 11162 (2009)
- [12] I. Shin, H. Seo, M. K. Son, J. K. Kim, K. Prabakar, and H. J. Kim, *Curr. Appl. Phys.*, **10**, S422 (2010)
- [13] K. H. Park and C. K. Hong, *Electrochem. Commun.* **10**, 1187 (2008)
- [14] J. Han, J. M. Chen, X. W. Zhou, Y. Lin, J. B. Zhang, and J. G. Jia, *Chinese Chem. Lett.* **19**, 1004 (2008)
- [15] M. Grätzel, *Curr. Opin. Colloid Interface Sci.*, **4**, 314 (1999)
- [16] J. R. Durrant and S. A. Haque, *Nature Mat.*, **2**, 362 (2003)
- [17] M. Grätzel, *Prog. Photovolt. Res. Appl.*, **8**, 171 (2000)

- [18] T. Miyasala and Y. Kijitori, *J. Electrochem. Soc.*, **151**, A1767 (2004)
- [19] M. Grätzel, *MRS Bull.*, **30**, 23 (2005)
- [20] C. J. Barbe, F. Arendse, P. Comte, M. Jirousek, F. Lenzmann, V. Shklover, and M. Grätzel, *J. Am. Ceram. Soc.*, **80**, 3157 (1997)
- [21] K. Kalyanasundaram and M. Grätzel, *Coord. Chem. Rev.*, **77** (1998)
- [22] M. K. Nazeeruddin, A. Kay, I. Rodicio, R. Humphrybaker, E. Muller, P. Liaka, N. Vlachopoulos, and M. Grätzel, *J. Am. Ceram. Soc.*, **115**, 6382 (1993)
- [23] G. P. Smestad and M. Grätzel, *J. Chem. Educ.*, **75**, 752 (1998)
- [24] D.S. Tsoukleris, I. M. Arabatzis, E. Chatzivasiloglou, A. I. Kontos, V. Belessi, M. C. Bernard, and P. Flaras, *Sol. Energy*, **79**, 422 (2005)
- [25] S. Karuppuchamy, K. Nonomura, T. Yoshida, T. Sugiura, and H. Minoura, *Solid State Ion.*, **151**, 19 (2002)
- [26] S. Karuppuchamy, D. P. Amalnerkar, K. Yamaguchi, T. Yoshida, T. Sugiura, and H. Minoura, *Chem. Lett.*, 78 (2001)
- [27] M. S. Wong, T. S. Yang, and C. B. Shiu, *Surf. Sci.*, **548**, 75 (2004)
- [28] S. B. Amor, G. Baud, J. P. Besse, and M. Jacquet, *Thin Solid Films*, **293**, 163 (1997)
- [29] M. Gomez, E. Magnusson, E. Olsson, A. Hagfeldt, S. E. Lindquist, and C. G. Granquist, *Sol. Energy Mater. Sol. Cells*, **62**, 269 (2000)
- [30] D. Dumitriu, *Appl. Catal. B-Environ.*, **25**, 83 (2000)
- [31] K. Okimura, *Surf. Coat. Technol.*, **135**, 186 (2001)
- [32] P. Zeman and S. Takabayashi, *Surf. Coat. Technol.*, **153**, 93 (2002)
- [33] D. Byun, *J. Hazard. Mater.*, **73**, 199 (2000)
- [34] D. R. Burgess, P. A. Morris, T. J. Anderson, and J. L. Hohman, *J. Cryst. Growth*, **166**, 763 (1999)
- [35] M. Paulose, K. Shankar, O. K. Varghese, G. K. Mor, and C. A. Grimes, *J. Phys.*

- D: Appl. Phys., **39**, 2498 (2006)
- [36] B. Tan and Y. Y. Wu, J. Phys. Chem. B, **110**, 15932 (2006)
- [37] Solaronix Website
- [38] M. Grätzel, Inorg. Chem., **44**, 6841 (2005)
- [39] T. Naoki and Y. Wang, Langmuir, **10**, 4574 (1994)
- [40] S. R. Brankovic, J. McBreen, and R. R. Adzic, Surf. Sci., **479**, L363 (2001)
- [41] A. Kay and M. Grätzel, Sol. Energy Mater. Sol. Cells, **44**, 99 (1996)
- [42] S. Cherian and C. C. Wamser, J. Phys. Chem. B, **104**, 3624 (2000)
- [43] J. Hagen, W. Schaffrath, P. Otschik, R. Fink, A. Bacher, H. W. Schmidt, and D. Haarer, Synth. Met., **89**, 215 (1997)
- [44] Y. X. Li, J. Hagen, W. Schaffrath, P. Otschik, and D. Haarer, Sol. Energy Mater. Sol. Cells, **56**, 167 (1999)
- [45] M. Okuya, K. Nakade, and S. Kaneko, Sol. Energy Mater. Sol. Cells, **70**, 425 (2002)
- [46] T. L. Ma, K. Inoue, H. Noma, K. Yao, and E. Abe, J. Photochem. Photobiol. A-Chem., **152**, 207 (2002)
- [47] G. Namutdinova, S. Sensfuss, M. Schrodner, A. Hinsch, R. Sastrawan, D. Gerhard, S. Himmler, and P. Wasserscheid, Solid State Ion., **177**, 3141 (2006)
- [48] P. Wang, S. M. Zakeeruddin, J. E. Moser, M. K. Nazeeruddin, T. Sekiguchi, and M. Grätzel, Nature Mater., **2**, 498 (2003)
- [49] W. Kubo, S. Kambe, S. Nakade, T. Kitamura, K. Hanabusa, Y. Wada, and S. Yanagida, J. Phys. Chem. B, **107**, 4374 (2003)
- [50] H. Usui, H. Matsui, N. Tanabe, and S. Yanagida, J. Photochem. Photobiol. A-Chem., **164**, 97 (2004)
- [51] S. Yanagida, M. Watanabe, H. Matsui, K. Okada, H. Usui, T. Ezure, and N. Tanabe, Fujikura Techn. Rev., **34**, 59 (2005)

- [52] W. Kubo, K. Murakoshi, T. Kitamura, S. Yoshida, M. Haruki, K. Hanabusa, H. Shirai, Y. Wada, and S. Yanagida, *J. Phys. Chem. B*, **105**, 12809 (2001)
- [53] R. Kawano, H. Matsui, C. Matsuyama, A. Sato, M. Susan, N. Tanabe, and M. Watanabe, *J. Photochem. Photobiol. A-Chem.*, **164**, 87 (2004)
- [54] S. S. Kim, K. W. Park, J. H. Yum, and Y. E. Sung, *J. Photochem. Photobiol. A-Chem.*, **189**, 301 (2007)
- [55] S. S. Kim, K. W. Park, J. H. Yum, and Y. E. Sung, *Sol. Energy Mater. Sol. Cells*, **90**, 283 (2006)
- [56] X. M. Fang, T. L. Ma, G. Q. Guan, M. Akiyama, and E. Abe, *J. Photochem. Photobiol. A-Chem.*, **164**, 179 (2004)
- [57] N. Papageorgiou, *Coord. Chem. Rev.*, **248**, 1421 (2004)
- [58] Y. Chiba, A. Islam, Y. Watanabe, R. Komiya, N. Koide, and L. Y. Han, *Japanese J. Appl. Phys. Part 2-Letters & Express Letters*, **45**, L638 (2006)
- [59] T. C. Wei, C. C. Wan, and Y. Y. Wang, *J. Phys. Chem. C*, **111**, 4847 (2007)
- [60] T. C. Wei, C. C. Wan, and Y. Y. Wang, *Appl. Phys. Lett.*, **88**, 103122 (2006)
- [61] Y. Saito, W. Kubo, T. Kitamura, Y. Wada, and S. Yanagida, *J. Photochem. Photobiol. A-Chem.*, **164**, 153 (2004)
- [62] Y. Saito, T. Kitamura, Y. Wada, and S. Yanagida, *Chem. Lett.*, **31**, 1060 (2002)
- [63] E. Ramasamy, W. J. Lee, D. Y. Lee, and J. S. Song, *Appl. Phys. Lett.*, **90**, 173103 (2007)
- [64] K. Imoto, K. Takahashi, T. Yamaguchi, T. Komura, J. Nakamura, and K. Murata, *Sol. Energy Mater. Sol. Cells*, **79**, 459 (2003)
- [65] R. Kikuchi, T. Hoshikawa, and K. Eguchi, *J. Electroanal. Chem.*, **588**, 59 (2006)
- [66] K. Suzuki, M. Yamaguchi, M. Kumagai, and S. Yanagida, *Chem. Lett.*, **32**, 28 (2003)
- [67] T. Kitamura, M. Maitani, M. Matsuda, Y. Wada, and S. Yanagida, *Chem. Lett.*,

1054 (2001)

- [68] N. Ikeda, K. Teshima and T. Miyasaka, *Chem. Commun.*, 1733 (2006)
- [69] S. Ito, N. L. C. Ha, G. Rothenberger, P. Liska, P. Comte, S. M. Zakeeruddin, P. Pechy, M. K. Nazeeruddin, and M. Grätzel, *Chem. Commun.*, **38**, 4004 (2006)
- [70] P. M. Sommeling, B. C. O'Regan, R. R. Haswell, H. J. P. Smit, N. J. Bakker, J. J. T. Smits, J. M. Kroon, and J. A. M. van Roosmalen, *J. Phys. Chem. B*, **110**, 19191 (2006)
- [71] N. G. Park, G. Schlichthorl, J. van de Lagemaat, H. M. Cheong, A. Mascarenhas, and A. J. Frank, *J. Phys. Chem. B*, **103**, 3308 (1999)
- [72] L. Y. Zeng, S. Y. Dai, K. J. Wang, X. Pan, C. W. Shi, and L. Guo, *Chin. Phys. Lett.*, **21**, 1835 (2004)
- [73] S. Ito, P. Liska, P. Comte, R. L. Charvet, P. Pechy, U. Bach, L. Schmidt-Mende, S. M. Zakeeruddin, A. Kay, M. K. Nazeeruddin, and M. Grätzel, *Chem. Commun.*, **41**, 4351 (2005)
- [74] S. Hore and R. Kern, *Appl. Phys. Lett.*, **87**, 263504 (2005)
- [75] T. Miyasaka, M. Ikegami, and Y. Kijitori, *J. Electrochem. Soc.*, **154** A455 (2007)
- [76] S. H. Kang, J.-Y. Kim, H. S. Kim, H.-D. Koh, J.-S. Lee, and Y.-E. Sung, *J. Photochem. Photobiol. A-Chem.*, **200**, 294 (2008)
- [77] H. Yu, S. Zhang, H. Zhao, G. Will, and P. Liu, *Electrochim. Acta*, **54**, 1319 (2009)
- [78] A. O. T. Patrocínio, L. G. Paterno, and N. Y. Murakami Iha, *J. Photochem. Photobiol. A-Chem.* **205**, 23 (2009)
- [79] J.-K. Lee, B.-H. Jeong, S.-I. Jang, Y.-G. Kim, Y.-W. Jang, S.-B. Lee, and M.-R. Kim, *J. Ind. Eng. Chem.* **15**, 724 (2009)
- [80] F. Huang, D. Chen, X. L. Zhang, R. A. Caruso, and Y. B. Cheng, *Adv. Funct. Mater.*, **20**, 1301 (2010)

- [81] L. Hu, S. Dai, J. Weng, S. Xiao, Y. Sui, Y. Huang, S. Chen, F. Kong, X. Pan, L. Liang, and K. Wang, *J. Phys. Chem. B*, **111**, 358 (2007)
- [82] L. Zhao, J. Yu, J. Fan, P. Zhai, and S. Wang, *Electrochem. Commun.*, **11**, 2052 (2009)
- [83] C. N. Rao, B.C. Satishkumar, A. Govindaraj, E. M. Vogl, and L. Basumallick, *J. Mater. Res.*, **12**, 604 (1997)
- [84] H. C. Zeng, S. M. Liu, L. M. Gan, L. H. Liu, and W. D. Zhang, *Chem. Mater.*, **14**, 1391 (2002)
- [85] Y. Bando, M. Zhang, and K. Wada, *J. Mater. Sci. Lett.*, **20** 167 (2001)
- [86] H. Imai, Y. Takei, K. Shimizu, M. Matsuda, and H. Hirashima, *J. Mater. Chem.*, **9**, 2971 (1999)
- [87] H. Imai, K. Shimizu, M. Matsuda, H. Hirashima, and N. Negishi, *J. Mater. Chem.*, **10**, 2005 (2000)
- [88] T. Kasuga, M. Hiramatsu, A. Hoson, T. Sekino, and K. Niihara, *Langmuir* **14**, 3160 (1998)
- [89] K.-M. Lee, V. Suryanarayanan, J.-H. Huang, K. R. J. Thomas, J. T. Lin, and K.-C. Ho, *Electrochim. Acta* **54** 4123 (2009)
- [90] J. Yu, J. Fan, and L. Zhao, *Electrochim. Acta*, **55** 597 (2010)
- [91] J. H. Park, S. Y. Jung, R. Kim, N. G. Park, J. Kim, and S. S. Lee, *J. Power Sources*, **194**, 574 (2009)
- [92] Y. J. Kim, M. H. Lee, H. J. Kim, G. Lim, Y. S. Choi, N. G. Park, K. Kim, and W. I. Lee, *Adv. Mater.*, **21**, 1 (2009)
- [93] L. Yang, Y. Lin, J. Jia, X. Xiao, X. Li, and X. Zhou, *J. Power Sources*, **182**, 370 (2008)
- [94] Y. Saito, S. Kambe, T. Kitamura, Y. Wada, and S. Yanagida, *Sol. Energy Mater. Sol. Cells* **83**, 1 (2004)



- [95] K. M. Lee, V. Suryanarayanan, and K. C. Ho, *Sol. Energy Mater. Sol. Cells*, **90**, 2398 (2006)
- [96] K. M. Lee, C. Y. Hsu, W. H. Chiu, M. C. Tsui, Y. L. Tung, S. Y. Tsai, and K. C. Ho, *Sol. Energy Mater. Sol. Cells*, **93** 2003 (2009)
- [97] Y. H. Lai, C. Y. Lin, J. G. Chen, C. C. Wang, K. C. Huang, K. Y. Liu, K. F. Lin, J. J. Lin, and K. C. Ho, *Sol. Energy Mater. Sol. Cells*, **94**, 668 (2010)
- [98] S. Brunauer, P. H. Emmett, and E. Teller, *J. Am. Chem. Soc.*, **60**, 309 (1938)
- [99] R. B. Anderson and W. K. Hall, *J. Am. Chem. Soc.*, **70**, 1727 (1984)
- [100] J. Jagiello, M. Thommes, J. Jagiello, and M. Thommes, *Carbon* **42**, 1227 (2004)
- [101] F. Kremer, A. Schonhals, and W. Luck, Broadband Dielectric Spectroscopy, Springer-Verlag, Berlin Germany, 2002
- [102] A. M. Sidorovich, *Ukrainian Physical Journal*, **29**, 8, 1175 (1984)
- [103] A. R. Hippel, Dielectrics and Wave, John Willey & Sons, N. Y., 1954
- [104] A. A. Volkov and A. S. Prokhorov, *Radiophys. Quantum Electron.*, **46**, 657 (2003)
- [105] D. Kim, P. Roy, K. Lee, and P. Schmuki, *Electrochem. Commun.*, **12**, 574 (2010)
- [106] Y. Chen, E. Stathatos, and D. D. Dionysiou, *J. Photochem. Photobiol. A-Chem.*, **203**, 192 (2009)
- [107] S. Kang, J.-S. Yu, M. Kruk, and M. Jaroniec, *Chem. Commun.*, **38**, 1670 (2002)
- [108] J. Jiu, F. Wang, M. Sakamoto, J. Takao, and M. Adachi, *Sol. Energy Mater. Sol. Cells* **87**, 77 (2005)
- [109] K. S. W. Sing, D. H. Everett, R. A. W. Haul, L. Moscou, R. A. Pierotti, J. Rouquerol, T. Siemieniowska, *Pure Appl. Chem.*, **57**, 603 (1985)
- [110] The University of Southern Maine, O=CHem Directory, Solvents
- [111] E. E. Dormidontova, *Macromolecules*, **37**, 7747 (2004)